ADVANCED CODED MODULATION FOR HIGH SPEED OPTICAL TRANSMISSION

by

Tao Liu

A Dissertation Submitted to the Faculty of the

DEPARTMENT OF ELECTRICAL AND COMPUTER ENGINEERING

In Partial Fulfillment of the Requirements

For the Degree of

DOCTOR OF PHILOSOPHY

In the Graduate College

THE UNIVERSITY OF ARIZONA

2016

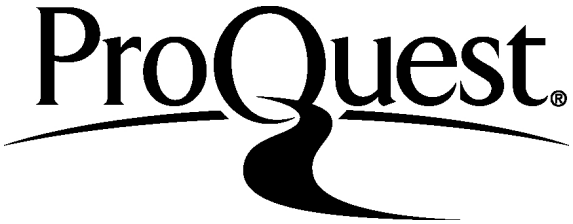

THE UNIVERSITY OF ARIZONA
GRADUATE COLLEGE

As members of the Dissertation Committee, we certify that we have read the dissertation prepared by Tao Liu, titled Advanced Coded Modulation For High Speed Optical Transmission and recommend that it be accepted as fulfilling the dissertation requirement for the Degree of Doctor of Philosophy.

_____ Date: 4/6/2016
Ivan B. Djordjevic

_____ Date: 4/6/2016
Milorad Cvijetic

_____ Date: 4/6/2016
Onur Ozan Koyluoglu

Final approval and acceptance of this dissertation is contingent upon the candidate's submission of the final copies of the dissertation to the Graduate College.

I hereby certify that I have read this dissertation prepared under my direction and recommend that it be accepted as fulfilling the dissertation requirement.

_____ Date: 4/6/2016
Dissertation Director: Ivan B. Djordjevic

STATEMENT BY AUTHOR

This dissertation has been submitted in partial fulfillment of the requirements for an advanced degree at the University of Arizona and is deposited in the University Library to be made available to borrowers under rules of the Library.

Brief quotations from this dissertation are allowable without special permission, provided that an accurate acknowledgement of the source is made. Requests for permission for extended quotation from or reproduction of this manuscript in whole or in part may be granted by the copyright holder.

SIGNED: Tao Liu

ACKNOWLEDGEMENTS

Numerous people have contributed to my success throughout this work, culminating in the realization of this dissertation. First and foremost, I would like to thank my family, my parents, for their continuous support over the years.

I have been extremely fortunate to work under the guidance of my amazing advisor, Dr. Ivan Djordjevic, who provided me the opportunity to participate in these exciting projects and who was always helping with sincere advice, guidance, support and time on my research, life and career path.

I would like to acknowledge Professor Milorad Cvijetic and Professor Onur Ozan Koyluoglu for their patience and expertise in reading through this work, Tami Whelan for without her I would never have surpassed the mountain of paperwork required for graduation, my colleagues, Yequn Zhang, Ding Zou, Changyu Lin, Xiaole Sun and Zhen Qu for their co-effort on the project, Dr. Murat Arabaci for his invaluable suggestions not only on this project, but also on other researches and sincere advice on life and career path.

TABLE OF CONTENTS

LIST OF FIGURES

ABSTRACT

In the recent years, the exponential Internet traffic growth projections place enormous transmission rate demand on the underlying information infrastructure at every level, from the long haul submarine transmission to optical metro networks. In recent years, optical transmission at 100 Gb/s Ethernet date rate has been standardized by ITU-T and IEEE forums and 400Gb/s and 1Tb/s rates per DWDM channel systems has been under intensive investigation which are expected to be standardized within next couple of years.

To facilitate the implementation of 400GbE and 1TbE technologies, the new advanced modulation scheme combined with advanced forward error correction code should be proposed. Instead of using traditional QAM, we prefer to use some other modulation techniques, which are more suitable for current coherent optical transmission systems and can also deal with the channel impairments. In this dissertation, we target at improving the channel capacity by designing the new modulation formats. For the first part of the dissertation, we first describe the optimal signal constellation design algorithm (OSCD), which is designed by placing constellation points onto a two dimensional space. Then, we expand the OSCD onto multidimensional space and design its corresponding mapping rule. At last, we also develop the OSCD algorithm for different channel scenario in order to make the constellation more tolerant to different channel impairments. We propose the LLR-OSCD for linear phase noise dominated channel and NL-OSCD for nonlinear phase noise dominated channel including both self-phase modulation (SPM) and cross-phase modulation (XPM) cases. For the second part of the dissertation, we target at probability shaping of the constellation sets (non-uniform signaling). In the conventional data transmission schemes, the probability of each point in a given constellation

is transmitted equally likely and the number of constellation sets is set to 2^n. If the points with low energy are transmitted with larger probability then the others with large energy, the non-uniform scheme can achieve higher energy efficiency. Meanwhile, this scheme may be more suitable for optical communication because the transmitted points with large probabilities, which have small energy, suffer less nonlinearity. Both the Monte Carlo simulations and experiment demonstration of both OSCD and non-uniform signaling schemes indicate that our proposed signal constellation significantly outperforms QAM, IPQ, and sphere-packing based signal constellations.

CHAPTER 0

INTRODUCTION

In the recent years, with the rapid growth in carrier-grade data-centric applications and services, and the general deployment of broadband wireless and wire line access networks, there has been a strong impetus for the DWDM network to upgrade from 10 Gb/s per channel to more spectrally-efficient 40 Gb/s or 100 Gb/s per channel transmission combined with Nyquist shaping [1]. In recent years, optical transmission at 100 Gb/s Ethernet data rate has been standardized by ITU-T and IEEE forums, while 400 Gb/s and 1 Tb/s rates per DWDM channel systems have been under intensive investigation which are expected to be standardized within next several years.

To facilitate the implementation of 400GbE and 1TbE technologies, we propose the use of advanced coded modulation scheme, which includes different advanced modulation formats. Instead of using traditional QAM, we prefer to use some other modulation techniques, which are more suitable for current coherent optical transmission system and can also deal with the channel impairments. In this dissertation, we target at improving the channel capacity by designing the new modulation formats. For the first part of the dissertation, we first describe the optimal signal constellation design algorithm (OSCD), [2]-[3] which is designed by placing constellation points onto a two dimensional space. Then, we expand the OSCD onto multidimensional space and design its corresponding mapping rule. At last, we also develop the OSCD algorithms for different channel scenarios in order to make the constellation more tolerant to different channel impairments. We propose the LLR-OSCD for linear phase noise dominated channel and NL-OSCD for nonlinear phase noise dominated channel including both self-phase modulation (SPM) and cross-phase modulation (XPM) cases. For the second part of the dissertation, we target at probability shaping of the constellation sets (non-uniform signaling). In the conventional data transmission schemes, the probability of each point in a given constellation is transmitted equally

likely and the constellation sets are set to 2^n. If the points with low energy are transmitted with larger probability then the others with large energy, the non-uniform scheme can achieve energy efficiency. Meanwhile, this scheme may be more suitable for optical communication because the transmitted points with large probability, which have small energy, suffer less fiber nonlinearity. Both the Monte Carlo simulations and experiment demonstration of both OSCD and non-uniform signaling scheme indicate that our proposed signal constellations significantly outperform QAM, IPQ, and sphere-packing based signal constellations.

This dissertation is organized as follows. Chapter 1 introduces the fundamental concept of the optimal signal constellation design and further investigates its performance through both Monte Carlo simulations and experiment demonstrations. Chapter 2 solves the problem of how to use the OSCD algorithm to design the constellation that can be more tolerant to target channel impairments. In this chapter, we introduce the LLR-OSCD and NL-OSCD for linear phase noise and nonlinear phase noise dominated channel. In chapter 3, we further expand the OSCD to DWDM system in order to make the resulting constellation formats more tolerant to cross phase modulation (XPM). Chapter 4 describes a different method that is called non-uniform signaling as well as its corresponding LDPC coded modulation scheme. At last, the conclusion and future work are summarized in Chapter 5.

CHAPTER 1

OPTIMUM SIGNAL CONSTELLATION DESIGN ALGORITHM

1.1 INTRODUCTION

From information theory we know that Gaussian distribution is optimum distribution for Gaussian channels [4]. For uncompensated fiber-optics link the resulting distribution is Gaussian-like, which motivates the use of Gaussian-like constellations. Upon compensation of fiber nonlinearities, chromatic dispersion and PMD, the equivalent channel model is Gaussian-like, again justifying the use of Gaussian-like constellations. When these assumptions are not applicable, the same algorithms proposed in this dissertation can still be used, but now based on optimum source distribution instead of Gaussian distribution.

1.1.1 Maximum Differential Entropy for Specified Variance

The problem of maximizing the differential entropy is a constrained optimization problem. The differential entropy of a random variable X is defined as:

$$\mathrm{h(X)} = -\int_{-\infty}^{\infty} f_X(x) log_2 f_X(x) dx. \tag{1.1}$$

We can associate with this probability density function $f_X(x)$ two constraints as:

$$\int_{-\infty}^{\infty} f_X(x)\, dx = 1, \tag{1.2}$$

and

$$\int_{-\infty}^{\infty} (x-\mu)^2 f_X(x)\, dx = \sigma^2 = constant, \tag{1.3}$$

where μ is the mean of X and σ^2 is its variance. The first constraint is a probability constraint, and the second constraint is the average power constraint

We use the method of Lagrange multipliers to solve this constrained optimized problem and set the function below as the Lagrangian function:

$$\int_{-\infty}^{\infty} [-f_X(x) log_2 f_X(x) dx + \lambda_1 f_X(x) + \lambda_2 (x-\mu)^2 f_X(x)] dx. \tag{1.4}$$

When the value of this function is stationary, the differential entropy $h(X)$ will attain its maximum value. The parameters λ_1 and λ_2 are known as Lagrange multipliers. That means h(X) is maximum only when the derivative of the Lagrangian

$$(d/df_X(x)) \int_{-\infty}^{\infty}[-f_X(x)log_2 f_X(x)dx + \lambda_1 f_X(x) + \lambda_2(x-\mu)^2 f_X(x)] = 0. \quad (1.5)$$

This yields the result

$$-log_2 e + \lambda_1 + \lambda_2(x-\mu)^2 = log_2 f_X(x) = (log_2 e) ln f_X(x) \quad (1.6)$$

where e is the base of the natural logarithm. Solving for $f_X(x)$, we get

$$f_X(x) = \exp\left[-1 + \frac{\lambda_1}{log_2 e} + \frac{\lambda_2}{log_2 e}(x-\mu)^2\right] \quad (1.7)$$

Note that λ_2 has to be negative so that the integrals of $f_X(x)$ and $(x-\mu)^2 f_X(x)$ with respect to x converge. Using 1.2, 1.3 and 1.7, we can solve λ_1 and λ_2 as

$$\lambda_1 = \frac{1}{2} log_2\left(\frac{e}{2\pi\sigma^2}\right) \quad (1.8)$$

and

$$\lambda_2 = -\frac{log_2 e}{2\sigma^2} \quad (1.9)$$

The desired form for $f_X(x)$ is therefore described as

$$f_X(x) = \frac{1}{\sqrt{2\pi}\sigma} \exp\left(-\frac{(x-\mu)^2}{2\sigma^2}\right) \quad (1.10)$$

The function above can be recognized as the probability density of a Gaussian random variable X of mean μ and variance σ^2. The maximum value of the differential entropy of such a random variable can be written as

$$\mathrm{h(X)} = \frac{1}{2} log_2(2\pi e\sigma^2) \quad (1.11)$$

So we can conclude that for a given variance σ^2, the Gaussian random variable has the largest differential entropy attainable by any random variable and the entropy of a Gaussian random variable X is uniquely determined by the variance of X (i.e., it is independent of the mean of X).

1.1.2 Maximum Mutual Information

For the additive Gaussian channel, the channel capacity is defined as the maximum of mutual information. With the theory described in Section 1.1.1, we can easily prove that the maximum capacity can be achieved when X is a Gaussian random variable.

The mutual information is defined as

$$\mathrm{I}(X;Y) \triangleq h(Y) - h(Y|X). \tag{1.12}$$

and the channel capacity is

$$\mathrm{C} \triangleq \max_{f(X)} I(X;Y) \tag{1.13}$$

We can calculate the $h(Y)$ and $h(Y|X)$ as

$$h(Y|X) = \frac{1}{2}\log\left(2\pi e\sigma_n^2\right) \tag{1.14}$$

and

$$h(Y)_{max} = \frac{1}{2}\log\left(2\pi e(\sigma_x^2 + \sigma_n^2)\right) \tag{1.15}$$

In formula 1.15, $h(Y)$ can be maximized when X is Gaussian variance, as described in Section 1.1.1. So we can also get the maximum channel capacity because the value of $h(Y|X)$ is determined by the channel only. At last, the conclusion is the optimum source distribution for Gaussian channels, such as ASE-noise-dominated channels and uncompensated links, is Gaussian.

1.2 Iterative Polar Quantization-Based Modulation (IPQ)

There are numerous studies aimed at non-uniform coded-modulation format in order to achieve channel capacity in high-speed optical communication systems. For instance, the optimized constellation can be obtained by using iterative polar quantization (IPQ) [5].

The disadvantage of IPQ constellation is that it is hard to expand to higher dimensional space. The vector quantization is more superior then the scalar one, while the polar quantization can be described as the optimal vector quantization (OVQ) in a two-dimensional space. But this problem is not that simple when moving to higher dimensional space. So we should invent new method of reasonable complexity that is applicable to higher dimensional space.

1.3 Optimal Signal Constellation Design Algorithm

In this section, we propose a polarization-multiplexed coded-modulation scheme based on signal constellations obtained by minimization of mean-square error (MSE) of signal constellation representing the source, for the optimum source distribution. The optimum source distribution is obtained by maximizing the mutual information, based on Arimoto-Blahut algorithm [4]. Therefore, these signal constellations are optimum in the minimum MSE (MMSE) sense, and the proposed algorithm can be named MMSE-optimum signal constellation design (MMSE-OSCD) algorithm. Although the algorithm is general, we demonstrate its efficiency by observing amplified spontaneous emission (ASE) noise dominated scenario. This scenario is realistic when coarse digital back-propagation (with reasonable small number of coefficients) is combined with sliding-window turbo equalization [5]. In addition, the distribution in uncompensated links upon electronic compensation of chromatic dispersion, PMD and SPM is Gaussian-like. Monte Carlo simulations indicate that signal constellations obtained by this algorithm significantly outperform conventional QAM signal constellations (~1 dB for 16-ary MMSE-OSCD constellation over 16-QAM). The proposed MMSE-OSCD also outperforms recently proposed IPQ-signal constellation [6], for medium signal constellation sizes.

The first stage in proposed algorithm is to use conventional Arimoto-Blahut algorithm to determine the optimum source distribution for a given optical channel. (This source distribution maximizes mutual information.) In the second stage, after initialization (for example, conventional QAM constellation can be used for initialization), we generate the samples from optimum source distribution and split them into clusters of points according Euclidean distance squared from constellation obtained in previous iteration. New constellation points are obtained as the center of mass of such obtained clusters. This procedure is repeated until convergence or until a predetermined number of iterations has been reached. It can be shown that this algorithm is optimum in MMSE sense [2].

The MMSE-OSCD algorithm can be formulated as:

1) Initialization: Choose an arbitrary auxiliary input distribution. Choose an arbitrary signal constellation as initial constellation and set the size of this constellation to *M*.
2) Apply the Arimoto-Blahut algorithm to determine optimum source distribution.
3) Generate long training sequences $\{x_j;\ j = 0, \dots, n-1\}$ from optimum source distribution, where *n* denotes the length of the training sequence used for signal constellation design. Let A_0 be the initial *M*-level signal constellation set of subsets of constellation points.
4) Group the samples from this sequence into *M* clusters. The membership to the cluster is decided by Euclidean distance squared of sample point and signal constellation points from previous iteration. Each sample point is assigned to the cluster with smallest distance squared. Given the *m*th subset (cluster) with *N* candidate constellation points, denoted as $\hat{A}_m = \{y_i\ ;\ i = 1, \dots, N\}$, find the minimum mean square error of partition $P(\hat{A}_m) = \{S_i\ ;\ i = 1, \dots, N\}$, as follows

$$D_m = D\left(\{\hat{A}_m, P(\hat{A}_m)\}\right) = n^{-1} \sum_{j=0}^{n-1} \min_{y \in \hat{A}_m} d(x_j, y) \tag{1.16}$$

where d is Euclidean distance squared between jth training symbol and symbol y being already in the subset (cluster). With $D(\cdot)$, we denoted the distance function. This step is illustrated in Figure 1.1.

5) If the relative error $|D_{m-1} - D_m|/D_m \leq e$, where e is the desired accuracy, the final constellation is described by $\{\hat{A}_m\}$. Otherwise continue.

6) Determine the new constellation points as center of mass for each cluster. With the mean square-error criterion, $x(S_i)$ is the Euclidean center of gravity or centroid given by

$$x(S_i) = \frac{1}{||S_i||}\sum_{j:x_j \in S_i} x_j \tag{1.17}$$

where $||S_i||$ denotes the number of training symbols in the region S_i as shown in Figure 2.1. If there is no training sequence in the region, set $x(S_i) = y_i$, the old constellation point. Define $\hat{A}_{m+1} = x(P(\hat{A}_m))$, replace m by $m + 1$, and go to step 3).

Repeat the steps 4)-6) until convergence.

As an illustration, in Fig. 1.2 we provide the signal constellations obtained for following signal constellation sizes: 16, 32, 64 and 128. The results are obtained for ASE noise dominated scenario.

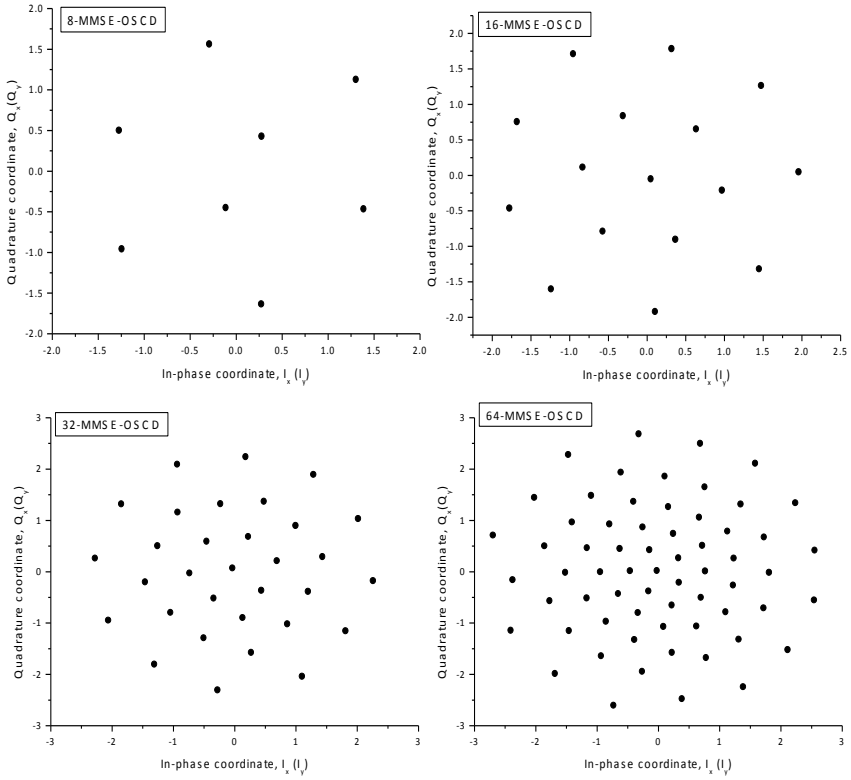

Figure 1.1 The MMSE-OSCD constellation sets.

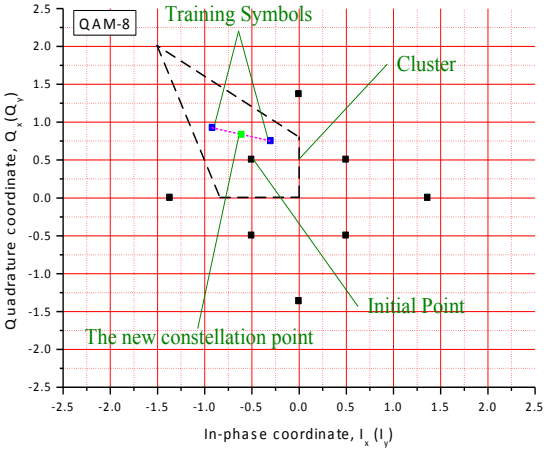

Figure 1.2 MMSE-OSCD algorithm illustrations.

Notice that these signal constellations remind to that of IPQ-signal constellations introduced in [5], except for the center point. Alternatively, someone may use IPQ-approach by

placing first single point in the origin and then apply the IPQ-procedure. Notice, however, that IPQ-procedure uses some approximations to come up with closed form solutions, which are valid assumptions for reasonable large signal constellation sizes. Therefore, it is a suboptimum solution for medium signal constellations' sizes. We will later show that signal constellations obtained by MMSE-OSCD algorithm significantly outperform IPQ-inspired signal constellations containing the point located in the origin.

1.4 Polarization Multiplexed LDPC Coded OSCD Scheme

The proposed polarization-multiplexed LDPC-coded scheme based on MMSE-OSCD signal constellations is depicted in Figure 1.3. There are $m_x + m_y$ independent sources, where subscripts x and y correspond to $x-$ and $y-$ polarizations, respectively. Since the configurations of LDPC-coded MMSE-OSCD transmitter (T_X) are identical for both polarizations, we provide full details only for x-polarization. The independent streams in x-polarization are encoded using $[N, K_X]$ binary LDPC codes of code rate $R_X = K_X/N$; and outputs of decoders are written row-wise into block-interleaver. The m_x bits taken from interleaver column-wise are used to select a coordinate from MMSE-OSCD 2^{m_x}-ary signal constellation implemented as a look-up-table (LUT). The LUT coordinates are after pulse shaping used as inputs to I/Q modulator (I/Q MOD). The independent polarization streams are combined by polarization beam combiner and transmitted over the system of interest. On receiver side, conventional polarization diversity receiver is used, whose outputs provide estimates of I and Q coordinates for both polarizations. Further, the course digital back-propagation is used, with small number of coefficients just to reduce the channel memory so that the complexity of sliding-window MAP equalizer that follows is not too high. The sliding-MAP equalizer provides

soft symbol log-likelihood ratios (LLRs), which are used to calculate bit LLRs, which are then passed to LDPC decoders. Further, the turbo equalization principle is used as explained in [7]. The LDPC codes are based on quasi-cyclic (QC) LDPC coded design of large girth, as described in [6]. The aggregate data rate of this scheme is $(m_X R_X + m_Y R_Y)R_S$, where R_S is the symbol rate.

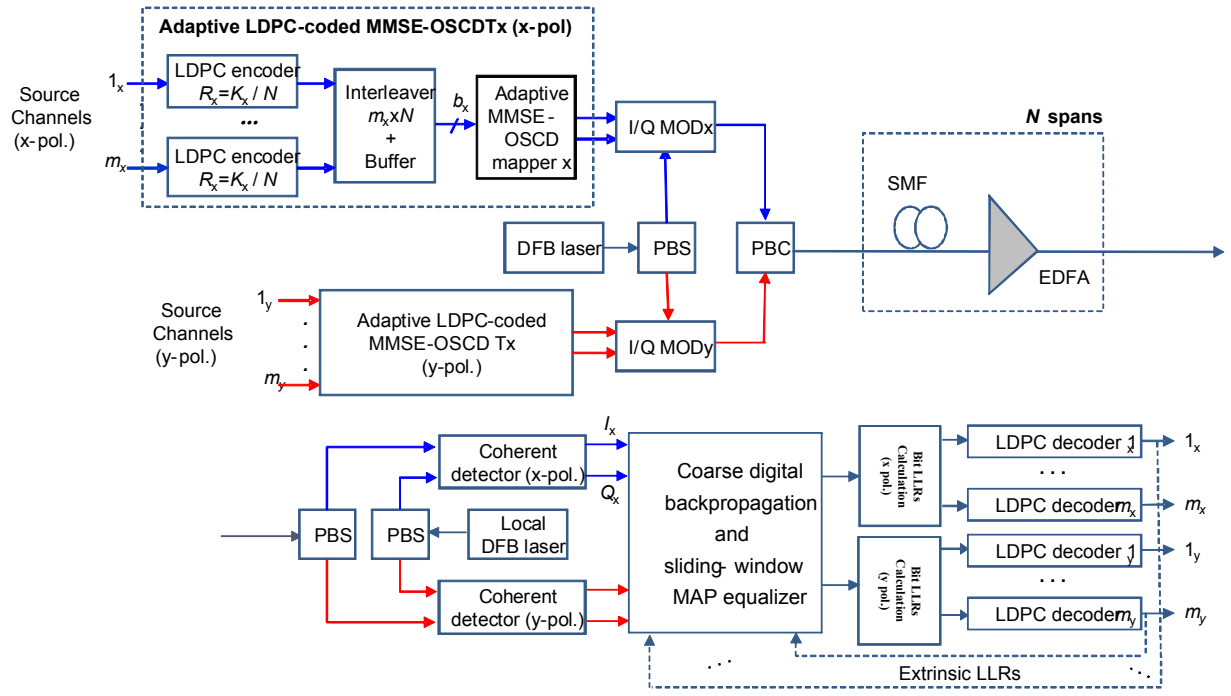

Figure 1.3 Polarization-division multiplexed LDPC-coded modulation scheme based on MMSE-OSCD signal constellations.

1.5 SIMULATION RESULTS

The results of Monte Carlo simulations for different signal constellation sizes of proposed MMSE-OSCD-algorithm based constellations are summarized in Fig. 1.4. All results of simulations are obtained for 25 LDPC decoder (inner) iterations and 3 MAP-LDPC decoder (outer) iterations, except for 16-ary MMSE-OCSD (i=20, o=5) curve, which is obtained for 20

inner and 5 outer iterations. It is evident that the largest improvement is obtained for 16-ary MMSE-OSCD. When measured at BER of 10^{-8}, the 16-ary MMSE-OSCD algorithm based signal constellation outperforms 16-QAM by almost 1 dB. The channel symbol rate was set to 31.25 GS/s, and QC LDPC (16935, 13550) of girth-8 and column-wieght-3 was used in simulations. The improvement of MMSE-OSCD over CIPQ and QAM decreases as the signal constellation size grows.

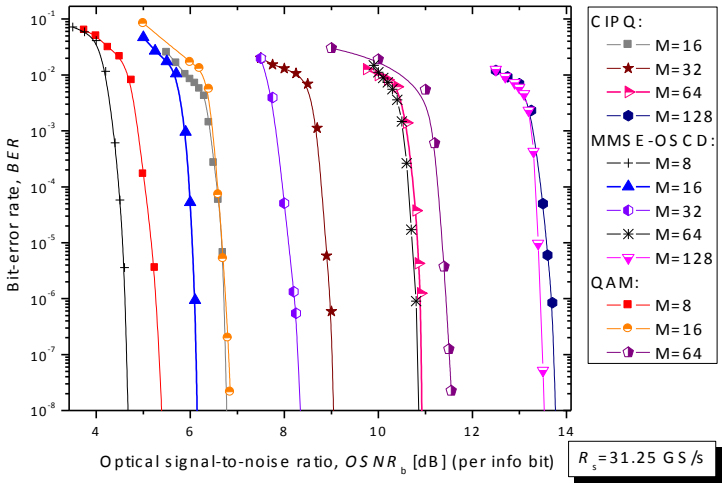

Figure 1.4 BER performance of proposed MMSE-OSCD algorithm based constellations against QAM and IPQ.

1.6 EXPERIMENTAL VERIFICATION

After the design of MMSE-OSCD, an ultra-long-haul experiment has been set up to study its performance over transoceanic distance. The experiment is targeting at testing the efficiency of the 8-OSCD. The system setup is described in Figure 1.6, where a total of 109 C-band DFB lasers spanning from 1529.88-1564.55nm and 91 L-band lasers spanning from 1572.40-1602.81nm at 40.2GHz spacing are independently modulated [8]. Each modulator produces 40Gbaud either 8-OSCD or regular 8-QAM, which are bit mapped through natural mapping or

optimal mapping from the output of an 8-ary irregular quasi-cyclic-LDPC (81126, 67605) encoder of girth 10. The testbed consists of 4×121.2km hybrid ultra-large- effective-areas/ultra-low-loss fibers, and gain equalizers. A 1-nm-bandwidth tunable optical filter has been placed in the front of a coherent receiver for selecting the channel of the interested to measure experimental performance. In the digital offline signal processing, nonlinear compensation (NLC) is applied using digital back propagation with one step per span to boost signal quality and shape the nonlinear noise into Gaussian-shape to avoid the potential error floor [9]. Blind phase searching algorithm has been used to recover the carrier phase in the stage of DD-LMS algorithm after the initial multi-modulus algorithm. The recovered symbols are then sent to non-binary LDPC decoder for counting post-FEC bit errors. Mix-domain FFT-based sum-product decoding algorithm is employed with 50 iterations or less. The details of system setup and DSP processing could be found in [10].

1.6.1 Measured Back to Back Performance

The coding performance of using regular and 8-OSCD modulation formats is compared in the BTB scenario as a function of pre-FEC Q-factor derived from bit-error counting and optical signal-to-noise ratio (OSNR) at 0.1nm resolution, as shown in Figure 1.5 (Note that 8-OSCD has been marked as optimized 8-QAM in this figure). Exponential fitting is used for extrapolating the measured BER data and thus estimating the FEC limit. As observed in Fig. 5(a), with the same LDPC codewords transmitted, the FEC limit achieved by using 8-OSCD is 4.05 dB at 20% overhead whereas 4.6 dB for regular 8QAM. Conforming to the findings in [2] there is 0.55 dB improvement in terms of pre-FEC limit when utilizing optimal nonbinary coded-8QAM due to the joint coded-modulation involving bit mapping, coding and modulation format. However, the

uncoded BER performance of 8-OSCD is worse than regular 8-QAM due to its smaller minimum Euclidean distance. As shown in Figure 1.5 (b), the FEC limits of optimized coded-8QAM and regular 8QAM are expected to be 15.3dB OSNR and 15.6dB, thus improving the receiver sensitivity by 0.3 dB after FEC decoding.

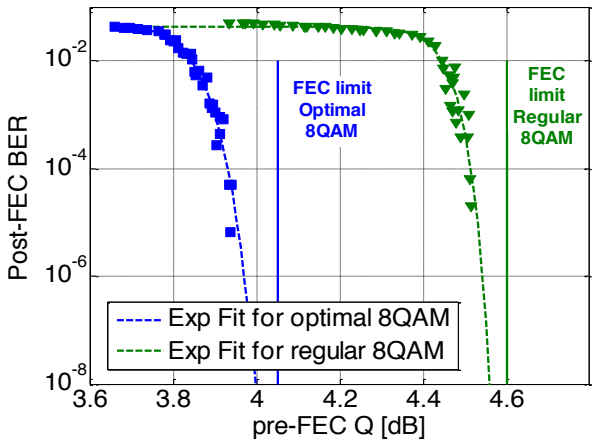

(a)

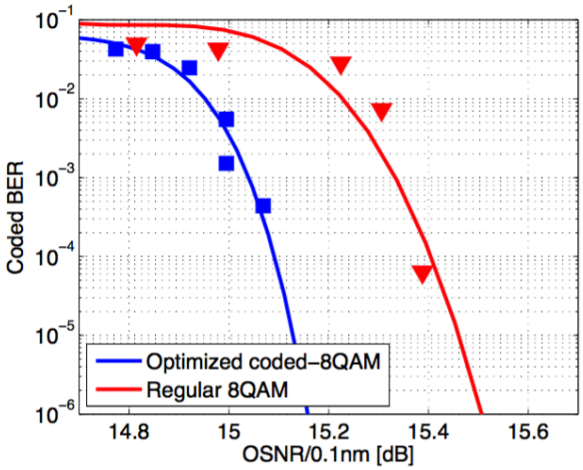

(b)

Figure 1.5 Experimental comparison of the coding performance between regular 8-QAM and 8-OSCD (a) coded BER versus pre-FEC Q and (b) coded BER versus OSNR.

1.6.2 Transmission Results

The received signal C + L-band spectra after 6780km is shown in Figure 1.6 (a). C and L-band

signals are transmitted in the opposite directions over the same fiber over 6780 km [11] to mitigate the nonlinear effects, such as Raman tiltering. The measured Q performance is plotted in Figure 1.6 (b) for the total 100 channels, accounting for dual-peak 400G. An average of 0.4dB in C-band and 0.8dB in L-band Q-factor improvement has been observed through NLC compared to CDC-only case. The different NLC improvement is caused because the channel power of C-band signals is slightly below the optimum channel power whilst L band is operated at a slightly above the optimum power to avoid excessive Raman interaction between bands [12]-[13], and also to minimize gain tilt at the L-band. In addition, the 8-OSCD could be benefited more from the NLC since the coded modulation has lower FEC limit and the improvement from NLC is sufficient to let the Q-factor moving away (to the right) from the LDPC water-fall region, thus avoiding bit errors. After NLC and BCJR equalization [14], the data of all channels in our experiment are recovered error free after FEC decoding.

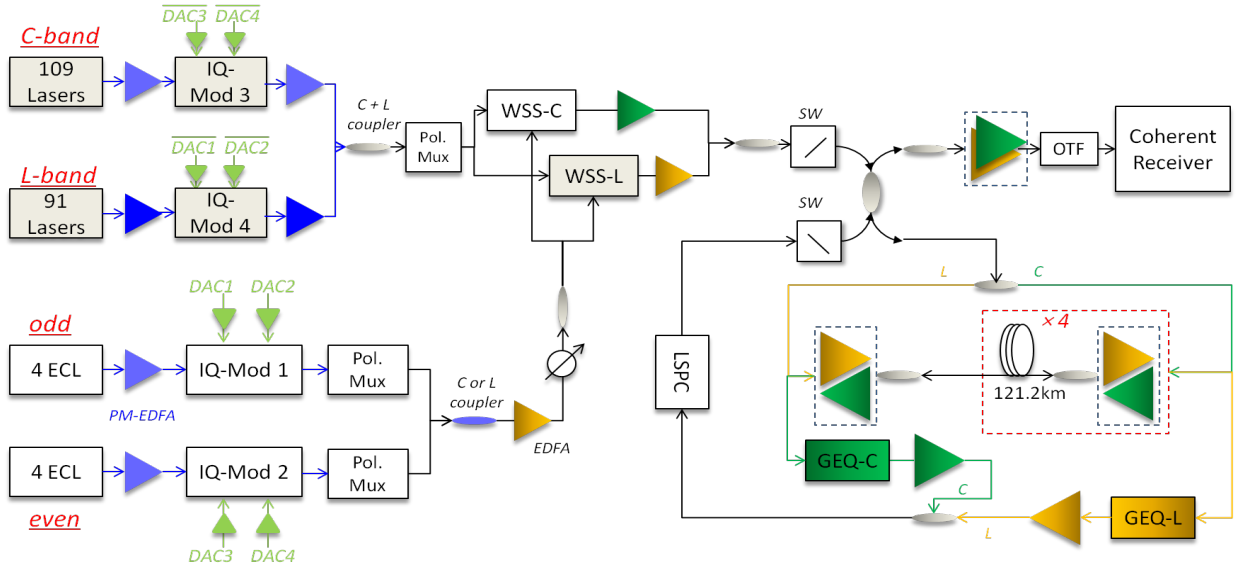

Figure 1.6 Experimental setup for evaluating the performance of optimized coded-8QAM.

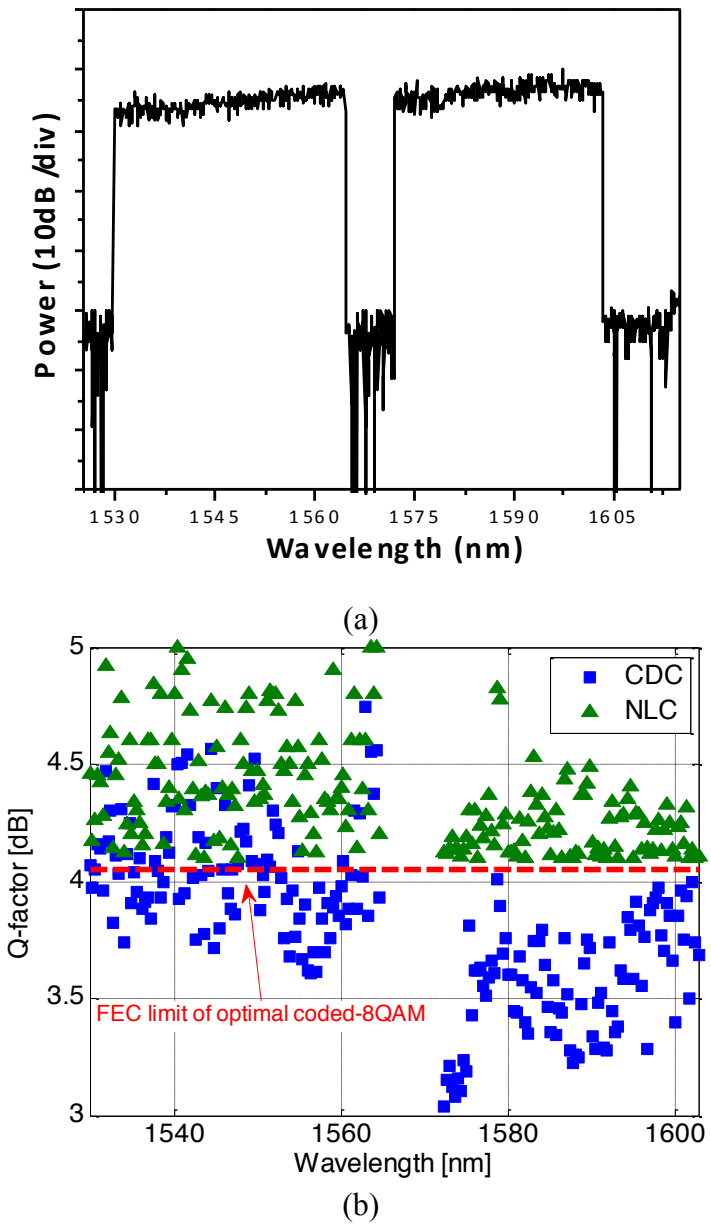

Figure 1.7 Experimental comparison of the coding performance between regular 8QAM and 8-OSCD (a) Received spectrum after 6787 km at 0.1 nm resolution; (b) Measured transmission performance for all channels with CDC and NLC after 6780km.

1.7 MULTIDIMENSIONAL OSCD

In order to get multidimensional OSCD constellations, we only need to expand the algorithm we

described above to the multidimensional space [15]-[16]. The first stage is also to use conventional Arimoto-Blahut algorithm for determining the N- dimensional optimum source distribution for a given optical channel, which is Gaussian distribution for ASE noise dominated channel. The properties of this source distribution achieve channel capacity. In the second stage, we first initialize the algorithm with a set of initial constellation points, for example the Cartesian product of QAM constellations or sphere-packing coordinates can be used for initialization. After the initialization stage, we generate the N- dimensional training sequences from optimum source distribution and split them into the clusters of points according to the Euclidean distance squared from constellation obtained in previous iteration. New constellation points are obtained as the center of mass of such obtained clusters. This procedure is repeated until convergence or until a predetermined number of iterations has been reached. It can be shown that this algorithm is optimum in MMSE sense [17].

The Figure 1.8 shows the 3D-8-ary OSCD signal constellation. The points form two tetrahedrons (blue and red) and they cross each other. The energy of every point is same and the points also show symmetric properties. On the other hand, the Figure 1.9 shows the 4D-8-ary OSCD signal constellation. The blue points denote the 2D projection of the first two coordinates and the green points represent the other two coordinates. It is evident that the points are symmetric to each other.

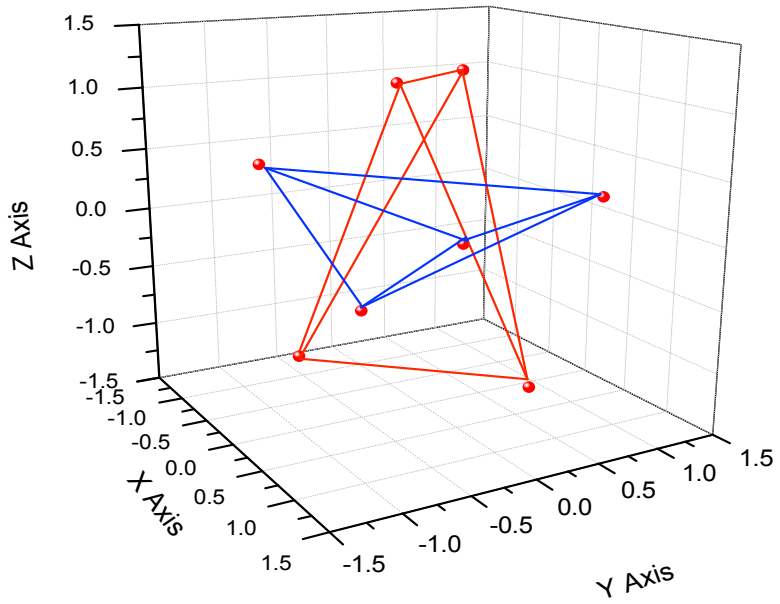

Figure 1.8 3D-8-ary OSCD Signal Constellation.

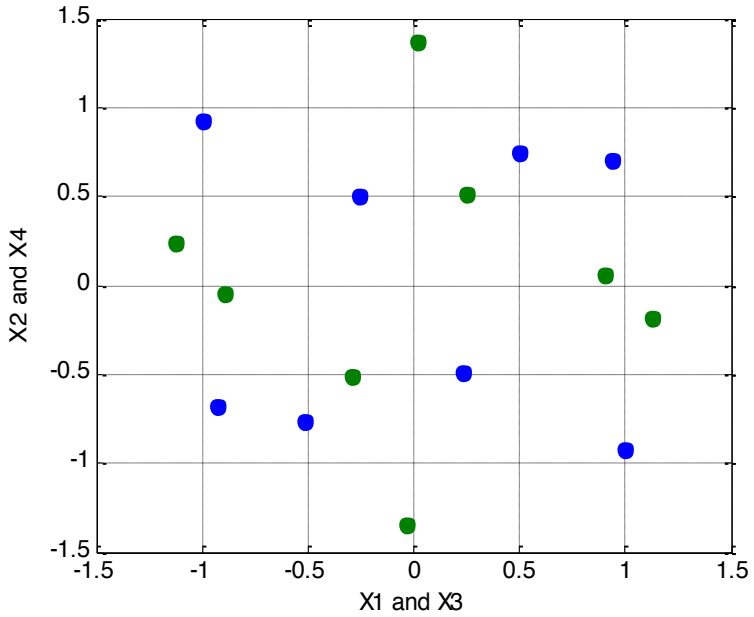

Figure 1.9 4D-8-ary OSCD signal constellation.

1.8 Optimal Mapping Rule for OSCD

The optimized mapping is preformed by maximizing the distance between detecting symbols with ideal a priori information at the demapper, by which we can achieve higher gain over

iterations for BICM-ID system. In our case, all the bits are perfectly known at the demapper, except for the bit to be detected, since only the extrinsic information is used [16], [18]. We denote the two symbols with the same known bits and different detecting bit as a detecting pair. The algorithm is to find the mapping in which each detecting pairs have large distance between each other and this distance should be larger than the minimum Euclidean distance of the constellation. This requirement should be satisfied for each detecting pair and for all detecting bits. In section 1.8, we propose the mapping method for low order OSCD constellation sets by using the cost function. This mapping method is only suitable for low order OSCD constellations. However, the binary switch algorithm should be used in order to find mapping method for arbitrary high order constellation sets. (Please refer to [16] for details about cost function and binary switch algorithm).

1.8.1 Mapping rule for 8 ary-2D-OSCD

The optimized mapping for 8-ary OSCD constellations is shown in the Figure 1.10. The distance between the detecting pairs for each detecting bits is also shown in Figure 1.10. The $x^{(i)}$ denotes the bit in the symbol and the white and black nodes with connection denote the detecting pair. We can easily see that the distance between the detecting pairs is larger than the minimum Euclidean distance (the distance between two central points). The proposed mapping method provides a good trade-off between performance with and without a priori information by maximizing the distance between symbol pairs.

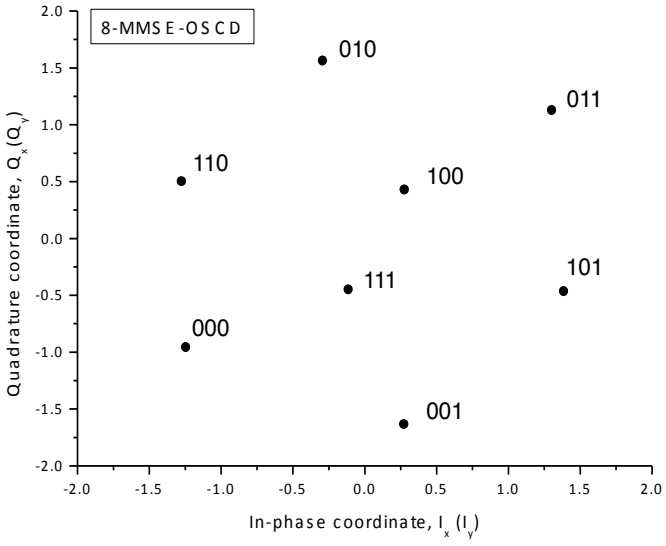

Figure 1.10 Optimal mapping for 8-OSCD.

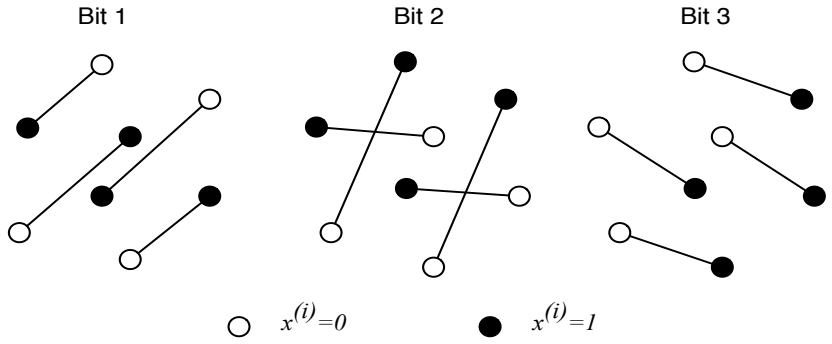

Figure 1.11 Detecting pairs for every bit position to be detected.

1.8.2 Mapping rule for 16 ary-3D-OSCD

The proposed mapping for 8-ary OSCD is an ideal case, which can satisfy all the conditions discussed above. Unfortunately, this ideal mapping does not exist for most constellation diagrams, but just for especially symmetric ones such as 8-ary OSCD. In order to find optimized mapping for common cases, an approximate method is introduced in [19], [20]. The cost function, which is shown below, is used in the algorithm.

$$f\left(\mu, \chi, \frac{E_s}{N_0}\right) = \frac{1}{m2^m} \sum_{i=1}^{m} \sum_{b=0}^{1} \sum_{s_k \in \chi_b^i} \sum_{\hat{s}_k \in \chi_{\bar{b}}^i} \exp\left(-\frac{E_s}{N_0} \|s_k - \hat{s}_k\|^2\right) \quad (1.18)$$

In (3), $\chi_b^i = \{s_k : s_k = \mu(c_k), c_k(i) = b, c_k \in \{0,1\}^m\}$ ($\mu(\cdot)$ is the mapping rule) denotes the signal constellation subset whose bit labels are $b \in \{0,1\}$ at position $i \in \{1, \dots, m\}$, E_s/N_0 is the symbol energy per power spectral density ratio, and $\|s_k - \hat{s}_k\|^2$ denotes Euclidean distance. Because the cost function is SNR dependent, SNR needs to be estimated by our expected BER performance. The optimized mapping is chosen by using the cost function to qualify each mapping rule for the constellation. However, the cost function cannot be applied to constellations with points more than 9 because of the huge optimization time. In 16 ary-2D-OSCD case, we use a pragmatic approach as follows. We first consider the inner circle of the constellation and implement the mapping as Gray mapping, which is shown as Figure 1.12 with black points. For the outer circle, we maximize the cost function to determine the mapping rule. The mapping rule for remaining red points is determined by maximizing the cost function.

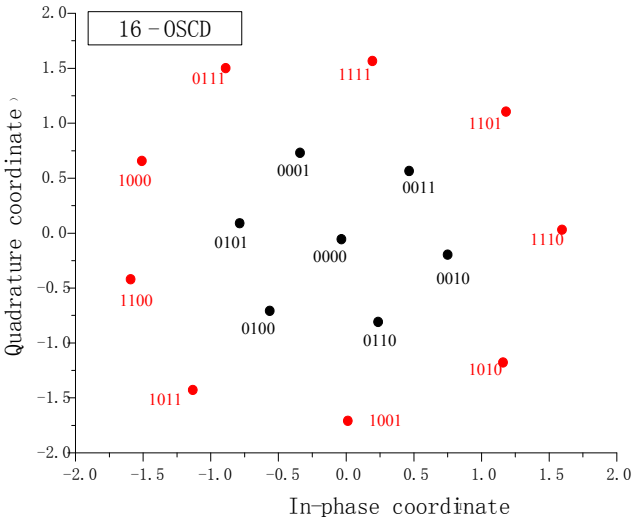

Figure 1.12 Optimal mapping for 16 ary-2D-OSCD.

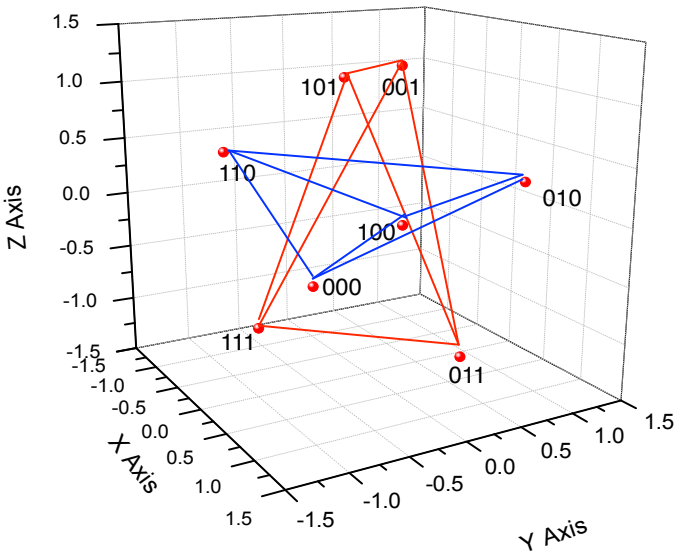

Figure 1.13 The optimized mapping rule for 16 ary-3D-OSCD.

1.8.3 Mapping rule for 8 ary-3D-OSCD

The mapping rule for 8-ary 3D-OSCD can be found by optimization of the cost function. We can easily find the optimal mapping with maximizing the cost function. The optimal mapping is shown in the Figure 1.13.

1.8.4 Mapping rule for 16 ary-3D-OSCD

In this case, again we cannot directly apply the cost function because of the long calculation time. On the other hand, we can see that the arrangement of the points at outermost layer in the 16-3D-OSCD is very similar to the 2D-8-OSCD, which is shown in the Figure 1.14. So we choose these points and implement the mapping rule as in our proposed 8-2D-OSCD optimized mapping rule and add 0 in the first bit position. Then the mapping rule for the remaining points can be determined by the cost function (1.18).

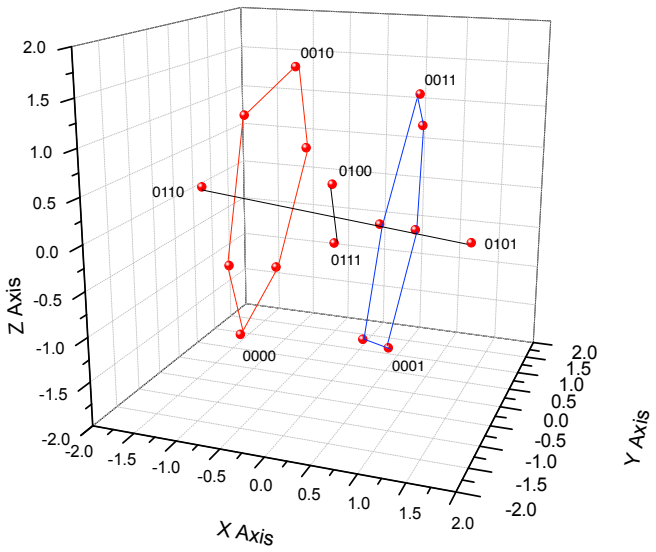

Figure 1.14 The optimized mapping rule for 16 ary-3D-OSCD.

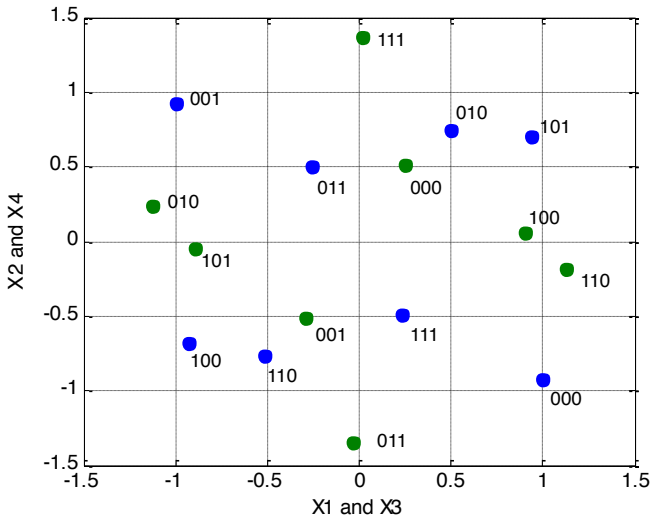

Figure 1.15 Optimal mapping for 8-ary-4D-OSCD.

1.8.5 Mapping rule for 8 ary-4D-OSCD

The mapping design for 8 ary-4D-OSCD is similar to the procedure described in the subsection 1.8.4. Because of the order of constellation is smaller than 9, we can directly apply the cost

function optimization. The optimum mapping rule is provided in Figure 1.15.

1.9 MULTIDIMENSIONAL OSCD CODED MODULATION SCHEME BASED ON PROPOSED MAPPING RULES AND SIMULATION RESULTS

The optimized mapping for OSCDs are studied for use in adaptive polarization-division multiplexed/mode-division multiplexed LDPC-coded modulation schemes, as illustrated in Figure 1.16, to enable both 400GbE and 1 TbE. The channel symbol rate was set to 31.25 GS/s, and QC LDPC (16935, 13550) code of girth-8 and column-weight-3 was used in simulations. All results are obtained for 20 LDPC decoder (inner) iterations and 3 MAP-LDPC decoder (outer) iterations and the LDPC-coded PDM 2D-OSCD results are summarized in Fig. 17, for the information symbol rate of 25 Gs/s. The QAM curves are generated by using natural mapping. It is clear that OSCD constellations outperform QAM constellations in both 16-ary and 8-ary cases. Also, the optimized mapping outperforms natural mapping for OSCD and the gap is almost 0.5 dB in 8-ary case. In 16-ary case, the gap is 0.6 dB. Note that in 16-ary OSCD case, the mapping is generated by the cost function that we introduced in Section 1.8, as the optimization by EXIT chart is intractable.

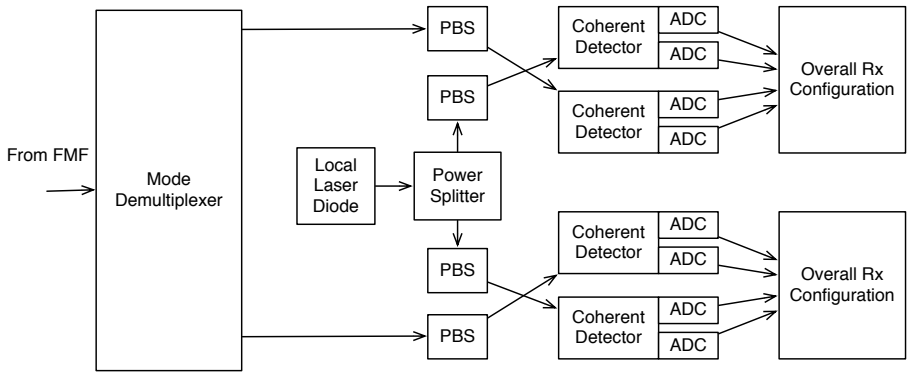

(a)

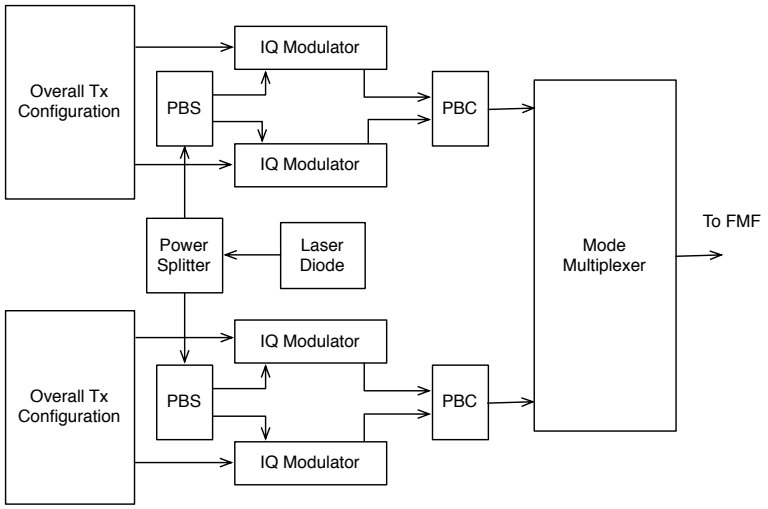

(b)

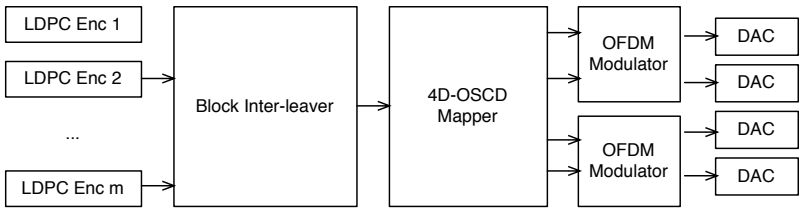

(c)

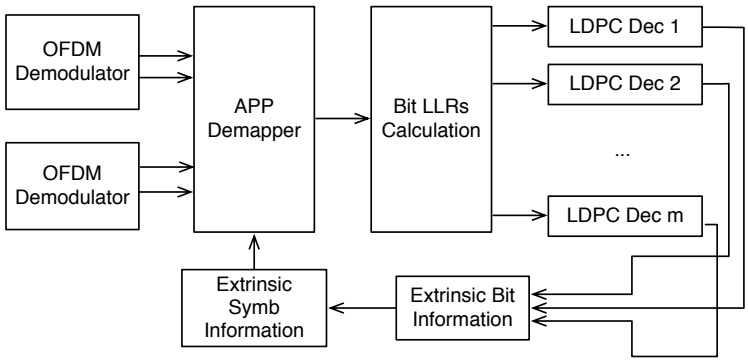

(d)

Figure 1.16 Schematic diagram of proposed LDPC-coded OFDM based on FMFs: (a) the transmitter setup, (b) the receiver setup, (c) details in overall Tx configuration, and (d) details in overall Rx configuration.

In the multidimensional case, the OSCDs should be combined with the OFDM [21], as

OFDM is effective in compensating mode coupling effects, in order to demonstrate the improvements that OSCD can bring together with optimized mapping rule. The corresponding scheme suitable for transmission over FMF in strong-coupling regime [19] is shown in Figure 1.16. Pilot-aided channel estimation technique is performed by inserting several pilot subcarriers in each OFDM symbol with a specific period. Least-square (LS) technique is used to estimate the pilot subcarrier coefficients in the first stage, then more advanced technique, the linear minimum mean-square error (LMMSE) estimator, is applied in second stage as follows:

$$\widehat{H}_{p,LMMSE} = R_{H_p,H_p}\left(R_{H_p,H_p} + \frac{\beta}{SNR}I\right)^{-1}\widehat{H}_{p,LS}, i \in \{0,1,\dots,N_p - 1\} \quad (1.19)$$

where $\widehat{H}_{p,LS}$ is the least-square estimate of H_p. $SNR = E\left|X_p(k)\right|/\sigma_n^2$ is the average signal-to-noise ratio, $\beta = E\left|X_p(k)\right|^2 E\left|1/X_p(k)\right|^2$ is a constant dependent on the signal constellation choice, and the covariance matrix is defined as $R_{H_p,H_p} = E\{H_p H_p^H\}$. This covariance matrix is obtained by transmitting several OFDM symbols as a preamble. The channel coefficients on data subcarriers are linearly interpolated from neighboring LMMSE pilot coefficients.

The original data stream are encoded by an LDPC code and written row-wise into a block-interleaver. Then the OSCD mapper accepts m bits from the block-interleaver column-wise and maps them to the 4D-OSCD constellation. In our case, there are four different parallel coordinate streams at each time signaling interval, as shown in Figure 1.16 (c). The first and the second coordinate streams are used as inputs to upper branch OFDM transmitter, while the third and the fourth as inputs to the lower branch OFDM transmitter. By using four identical I/Q modulators, the OFDM symbols are converted to optical domain with two different spatial modes [see Figure 1.16 (d)]. The OFDM transmitter inserts pilot in specific position and performs IFFT operation and then forwards the outputs to DACs [see Figure 1.16 (c)]. At the

receiver side, received samples are forwarded to OFDM demodulator, after coherent detection, whose output represents the estimated OSCD symbols. Then we perform the iterative decoding with APP demapper and LDPC decoder, which is shown in Figure 1.16 (d). The simulation result of 2D case of the different mapping of OSCDs is shown in Figure 1.17. The optimized mapping can further improve the performance by 0.3dB.

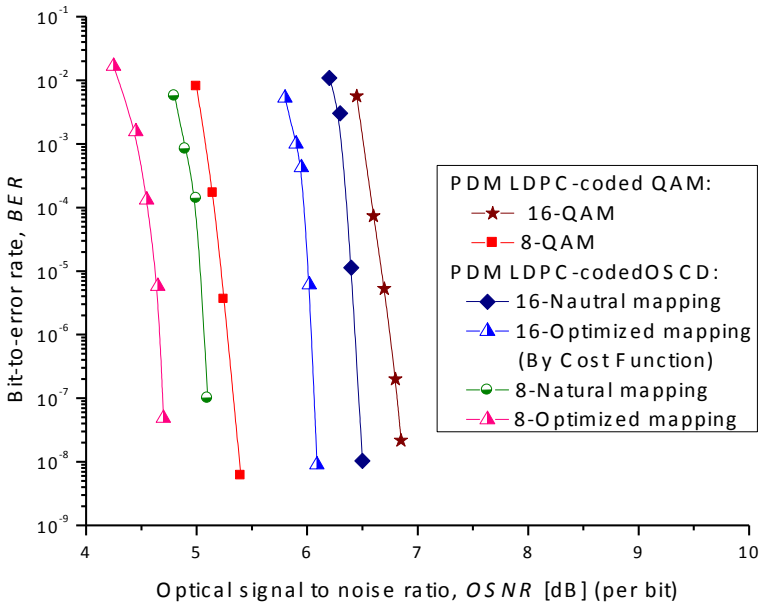

Figure 1.17 BER performance for optimal mapping rules of LDPC-coded PDM 2D-OSCDs.

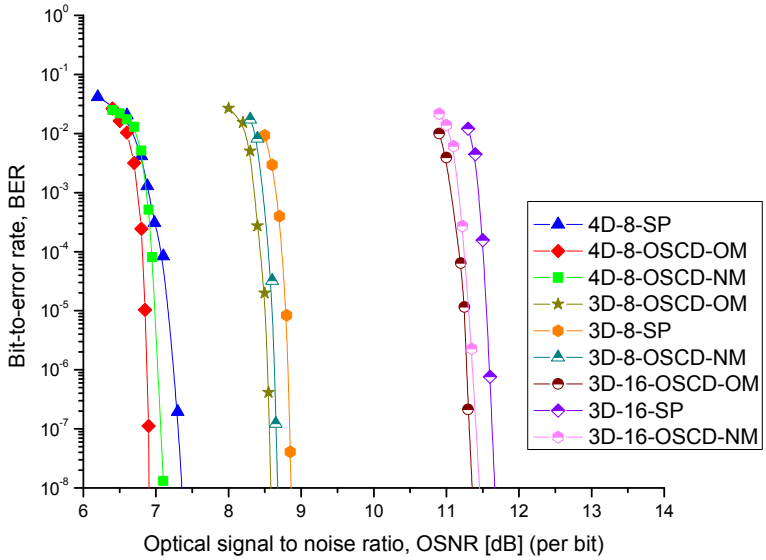

Figure 1.18 BER performance for optimal mapping rules of ND-OSCDs for MDM in FMF applications.

The component LDPC code used in simulation is quasi-cyclic LDPC (16935, 13550) code with code rate 0.8, as described above. In simulations, 20 inner iterations and 5 outer iterations between a posteriori probability (APP) demapper LDPC decoder are used [22]. The OFDM system parameters are chosen as follows: the number of subcarriers is set to 2048, out of them 64 are used as pilots. Cyclic extension is set to 128 samples, in order to accommodate for mode dispersion. LMMSE pilot estimator and linear interpolation are jointly used for channel estimation and compensation. The number of FMF modes is set to four. In simulations, four OFDM bands with 50 Giga symbols/s each (corresponding to 40 Giga symbols/s in effective information rate per band) have been used. (For additional details of this FMF scheme, please refer to ref. [19]) This scheme is suitable for multi-Tb/s serial optical transport. Monte Carlo simulation results are summarized in Figure 1.18, where NM, OM and SP stand for natural mapping, optimal mapping and sphere packing constellations. It is clear to see that our proposed

mapping rules perform the best among different schemes and the gap is 0.2 dB when compared to the natural mapping for 3D 8-ary-OSCD and 0.5 dB when compared to the sphere packing constellation.

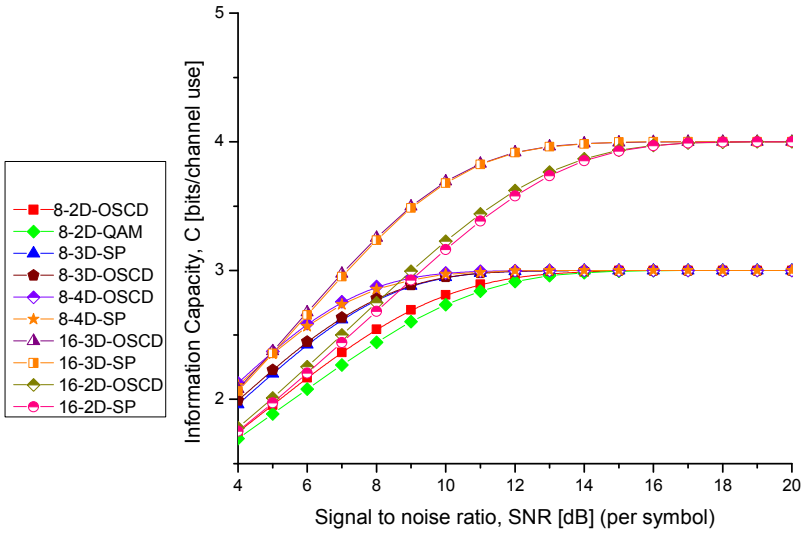

Figure 1.19 Information capacities of OSCD constellations against QAM and SP information capacities.

In order to illustrate the basic criterion for OSCD constellation, which is maximizing the channel capacity, we also provide information capacities for proposed signal constellations and compare them against that of QAM, and sphere packing constellations that are marked as SP. The results (not for BICM-ID system) are summarized in Figure 1.19. It is clear from figure, that our proposed OSCD constellations outperform QAM and SP constellations for all constellation sizes.

1.10 CONCLUSION

In this chapter, we have introduced the optimal signal constellation design algorithm with the simulation verification and experimental demonstration. Meanwhile, we also expand OSCD to

multidimensional case and discuss its corresponding mapping rule. By using the OSCD method, we can bring some properties of the Gaussian source to the small constellation sets and make the source input to channel to be Gaussian-like [23]. The OSCD algorithm is very flexible and can be expand to many cases. In next two chapters, we will introduce how to use OSCD algorithm to design the constellation that is more tolerant to certain channel impairments. For the OSCD family, please refer to [15] for feedback channel capacity inspired OSCD (FCC-OSCD), [24] for the OSCD designed for chromatic dispersion channel, [25] [26] for the OSCD mapping design and EXIT chart analysis and [27] for the OSCD combining with CO-OFDM.

CHAPTER 2

OPTIMAL SIGNAL CONSTELLATION DESIGN FOR PHASE ERROR DOMINATED CHANNEL

2.1 INTRODUCTION

The fiber nonlinearities can be considered as one of the most important factor in coherent long-haul optical transmission system [28]. Due to fiber Kerr nonlinear effects, the refractive index of optical fiber increases with optical intensity to slightly slow down the propagation speed, inducing intensity depending nonlinear phase shift, which includes the nonlinear phase noise (NLPN) because of the noise component in optical intensity introduced by amplifier [29]. In order to improve the performance of the long-haul optical transport systems with coherent detection, the nonlinear phase noise should be considered in order to increase data rates of future optical transmission system.

The optimal design of a signal constellation, i.e., placing M points in the complex plane such that symbol error probability (SEP) or a specific criterion is minimized under an average or peak power constraint, is a classical problem in communication theory [30]. However, only few are known about the constellation design for optical channel with nonlinear effects. A maximum likelihood (ML) detector for phase-shift keying modulated signals and two-stage detector for 16-QAM constellation has been proposed by Lau and Kahn [31]. Lotfollah has proposed 16-point ring constellation sets for combating the effect of NLPN [32]. Also, design of APSK constellations for coherent optical channels with NLPN is proposed by Christian in [33]. Although these methods can achieve better SEP performance, there is no consideration about an overall algorithm used to design the optimal constellation in presence of phase noise.

In this chapter, a new optimal constellation design algorithm is proposed which is applicable to coherent detection system in presence of linear or nonlinear phase noise. As an extension of the optimum constellation design algorithm (OSCD), which is introduced in [2], the proposed algorithm uses the cumulative log-likelihood function instead of the Euclidian distance,

which is applicable to both linear and nonlinear phase noise-dominating scenarios. The optimum source distribution used in the algorithm is generated by maximizing the channel capacity based on well-known Arimoto-Blahut algorithm [34]. In this scheme, the proposed algorithm can interact with channel impairments and log-likelihood function calculation by using same criterion. Also, an LDPC coded modulation scheme [35] suitable for use in combination with constellations obtained by this algorithm is proposed. Monte Carlo simulations indicate that the signal constellation obtained by our new algorithm outperforms corresponding QAM significantly in both linear and nonlinear phase noise dominated channel. Also, the new constellation set performs better than original OSCD constellation sets, which are obtained by the criterion of Euclidean distance.

2.2 CHANNEL MODEL

In this section, we introduce the equivalent coherent optical channel mode for both linear and nonlinear channel.

2.2.1 Coherent Optical Channel Dominated by Linear Phase Noise

The equivalent channel model for coherent detection, upon compensation of linear and nonlinear impairments and CPE, can be represented as:

$$r_k = s(a_k, \theta_k) + z, \quad r_k = [r_k^{(1)} \dots r_k^{(i)} \dots r_k^{(N)}]^T \tag{2.1}$$

$$s(a_k, \theta_k) = e^{j\theta_k}[a_k^{(1)} \dots a_k^{(i)} \dots a_k^{(N)}]^T, \qquad z_k = [z_k^{(1)} \dots z_k^{(i)} \dots z_k^{(N)}]^T \tag{2.2}$$

where $r_k^{(i)}$ is the ith component of observation vector at kth symbol interval, $a_k^{(i)}$ is the ith coordinate of transmitted symbol (at kth symbol interval), and z is the corresponding noise vector (with Gaussian-like distribution of components). The θ_k denotes the residual phase error

(at kth time instance) due to laser phase noise, nonlinear phase noise and imperfect CPE. In polarization-division multiplexing (PDM), Equation (2.1) and (2.2) correspond to either x- or y-polarization state. In 4-D signaling, the components above represent projections along in-phase and quadrature basis functions corresponding to x- and y- polarization. The model above is applicable to few-mode fiber (FMF) applications as well. For instance, to describe the laser phase noise and imperfect CPE, the Wiener phase noise model can be used:

$$\theta_k = (\theta_{k-1} + \Delta\theta_k) \bmod 2\pi \tag{2.3}$$

where $\Delta\theta_k$ is zero-mean Gaussian process of variance $\delta_{\Delta\theta} = 2\pi\Delta f T_s$. With T_s denoting the symbol duration and Δf denoting either linewidth or frequency offset. The cyclic slips can also be modeled by Markov-like process of certain memory. The probability density function (PDF) of the phase increment in (2.3) is given by

$$p_{\Delta\Theta}(\Delta\theta_k) = \sum_{n=-\infty}^{\infty} p(0, \delta_{\Delta\theta}^2, \Delta\theta_k - n2\pi) \tag{2.4}$$

where $p(0, \delta_{\Delta\theta}^2, \Delta\theta_k - n2\pi)$ denotes the Gaussian PDF of zero-mean, variance $\delta_{\Delta\theta}^2$, and argument $\Delta\theta_k - n2\pi$. The resulting noise process is Gaussian-like with the power spectral density of N_0 so that the corresponding conditional probability density function is given by:

$$p_R(r|a_k, \theta_k) = e^{-\frac{j||r_k - s(a_k,\theta_k)||^2}{N_0}}/(\pi N_0) \tag{2.5}$$

For non-Gaussian channels, we will need to use the method of histograms to estimate the conditional probability density function $p_R(r|a_k, \theta_k)$. Note that j denotes the imaginary unit.

2.3 COHERENT OPTICAL CHANNEL DOMINATED BY NONLINEAR PHASE NOISE

In this case, our channel model is nonlinear phase noise model with discrete amplification for the finite number of fiber spans. When the optical signal is periodically amplified by EDFAs, the nonlinear phase noise is unavoidably added to the optical signal and accumulated as the number spans increases. For convenience, we consider the discrete memoryless channel model, which is introduced in [28] and can be described as follows:

$$Y = (X + Z)e^{-j\Phi_{NL}} \tag{2.6}$$

where $X \in \mathcal{X}$ is the channel input, Z is the total additive noise, and Y is the channel observation. (In (2.6) j denotes the imaginary unit.) In each fiber span, the overall nonlinear phase shift Φ_{NL} is given by

$$\Phi_{NL} = \int_0^L \gamma P(z)dz = \gamma L_{eff} P \tag{2.7}$$

where P is the launch power and γ is the nonlinear Kerr-parameter. For a fiber span length of L with attenuation coefficient of α, the power evolution is described as $P(z) = Pe^{-\alpha L}$ and the effective length is defined as

$$L_{eff} = \frac{1 - e^{-\alpha L}}{\alpha} \tag{2.8}$$

For a system with N_A fiber spans, the overall nonlinear phase noise is given by:

$$\Phi_{NL} = \gamma L_{eff}\left\{|E_0 + n_1|^2 + |E_0 + n_1 + n_2|^2 + \cdots + \left|E_0 + n_1 + \cdots + n_{N_A}\right|^2\right\} \tag{2.9}$$

where E_0 is the baseband representation of the transmitted electric field, n_k is independent identically distributed zero-mean circular Gaussian random complex variable with variance δ_0^2.

The total additive noise ate the end of all fiber segments has the variance $\delta^2 \triangleq E[Z^2] = 2N_A\delta_0^2$ and can be calculated as [36]-[37]

$$\delta^2 = 2n_{sp}h\nu\alpha\Delta\nu N_A\, L \tag{2.10}$$

where all parameters are summarized in the Table 2.1 [31].

In this channel model, the variance of the phase noise is dependent on the channel input and the channel is specified by the number of spans, transmission length, and the launch power. In Figure 2.1, we show the received scatter plots for 16-QAM constellation with $K = 25$, $L = 2000$km for different power P. The *K* and *L* denotes the number of spans and total length.

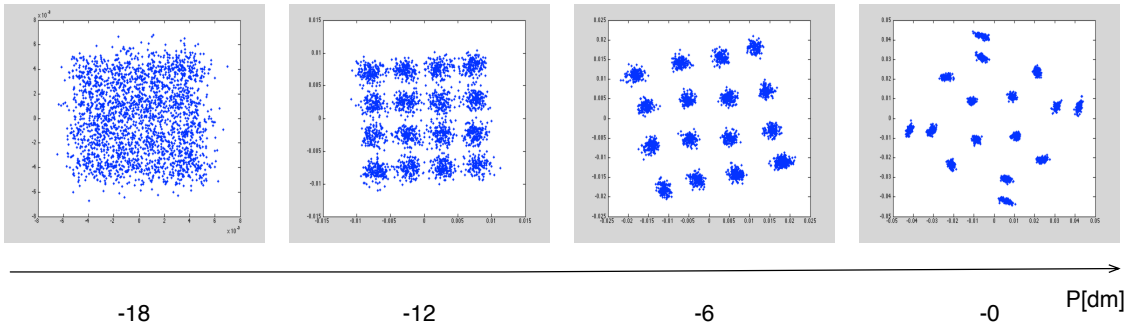

Figure 2.1 Scatter plots of received signal with 16-QAM constellation, L=2000km.

Table 2.1. Parameter of the Channel

Symbol	Typical value	The name of the parameter/constant
γ	$1.2\ W^{-1}\ km^{-1}$	Nonlinear Kerr-parameter
n_{sp}	1.41	Spontaneous emission factor
h	$6.626\times10^{-34}\ J\cdot s$	Planck's constant
ν	1.936×10^{14} Hz	Optical carrier frequency
α	$0.0578\ km^{-1}$	Fiber loss
$\Delta\nu$	42.6 GHz	Optical bandwidth

2.4 Optimal Signal Constellation Design for Phase Noise Dominated Channel

In the presence of phase noise, we can use an algorithm similar to OSCD algorithm [2], but now changing the optimization criterion. Instead of minimizing the mean square error, we define the cumulative log-likelihood function and get the optimal signal constellation that maximizes this function. Namely, the Euclidean distance receiver is optimum only for the AWGN channel. The starting point in the algorithm is to use the conventional Arimoto-Blahut algorithm to determine the optimum source distribution for the phase noise channel, and then generate the constellation samples from this source. Then we run our proposed algorithm, named here LLR-OSCD algorithm. The LLR-OSCD algorithm can be formulated as follows.

1) Initialization: Choose the signal constellation that will be used for initialization of size M.
2) Generate the training sequence from the optimum source distribution, denoted as $\{x_j;\ j = 0, \dots, n-1\}$.
3) Group the samples from this sequence into M clusters. The membership to the cluster is determined based on LLR of sample point and candidate signal constellation points from previous iteration. Each sample point is assigned to the cluster with the largest LLR. Given the mth subset (cluster) with N candidate constellation points, denoted as $\widehat{A}_m = \{y_i\ ;\ i = 1, \dots, N\}$, find the minimum mean square error of partition $P(\widehat{A}_m) = \{S_i\ ;\ i = 1, \dots, N\}$, as follows

$$LL_m = LL\left(\left\{\widehat{A}_m, P\left(\widehat{A}_m\right)\right\}\right) = n^{-1}\sum_{k=0}^{n-1}\max_{y\in\widehat{A}_m} LL(x_k, y) \tag{2.11}$$

The function $LL(x_j, y)$ is the cumulative log-likelihood function defined as

$$\mathrm{LL}(\mathrm{x_k}, \mathrm{y}) = \frac{1}{\mathrm{NS}} \sum_{\mathrm{i}=1}^{\mathrm{NS}} - \frac{\left\{\mathrm{x_{k1}} - \mathrm{Re}\left[(\mathrm{y_1} + \mathrm{y_2 j})\mathrm{e}^{-\mathrm{j}\times \mathrm{PN_i}}\right]\right\}^2 + \left\{\mathrm{x_{k2}} - \mathrm{Im}\left[(\mathrm{y_1} + \mathrm{y_2 j})\mathrm{e}^{-\mathrm{j}\times \mathrm{PN_i}}\right]\right\}^2}{2\delta^2} \tag{2.12}$$

where NS denotes the number of phase noise samples and the corresponding phase noise sample is denoted as $\mathrm{PN_i}$. $\mathrm{x_{k1}}$ and $\mathrm{x_{k2}}$ denote the first and second coordinates of the point $\mathrm{x_k}$. Similarly, $\mathrm{y_1}$ and $\mathrm{y_2}$ denote the coordinates of the received point y. The equation above is applicable to two-dimensional (2D) signal constellation design, but it can straightforwardly be generalized for arbitrary dimensionality.

4) Determine the new signal constellation points as center of mass for each cluster.

Repeat the steps 2)-3) until convergence.

The $\mathrm{PN_i}$ can be generated by target channel model introduced in section 2 for both linear and nonlinear phase noise case. That is to say, if $\mathrm{PN_i}$ is generated by linear phase noise model, then the resulting constellation is obtained for linear phase noise dominated scenario. Meanwhile, if $\mathrm{PN_i}$ is generated by nonlinear phase noise model, the result is obtained for nonlinear phase noise dominated scenario. The number of noise sample is chosen as 50 and the number of training sequence is 10^4 for 8-ary constellation and 10^5 for 16-ary constellation. We use QAM constellation as start point in our case.

As an illustration, in Figure 2.2 we provide the result of the proposed algorithm. The proposed constellations, which can be named as LLR-OSCD, for linear phase noise model are shown in Figure 2.2 (a), by setting the frequency offset × symbol duration product to 10^{-3}. Meanwhile, the constellation, which is called NL-OSCD, for nonlinear phase noise is also shown in Figure 2.2 (b). The result is generated at launch power of –6 dB, and transmission length of 2000 km.

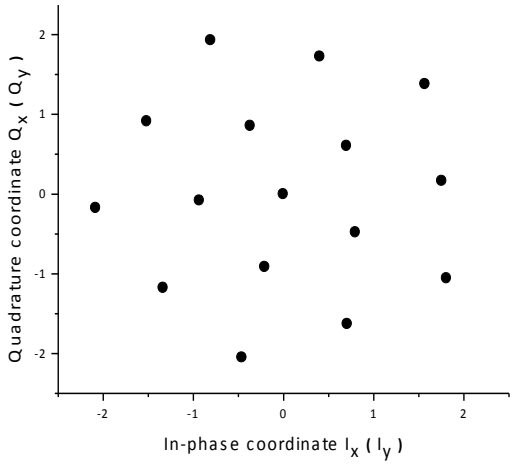

(a)

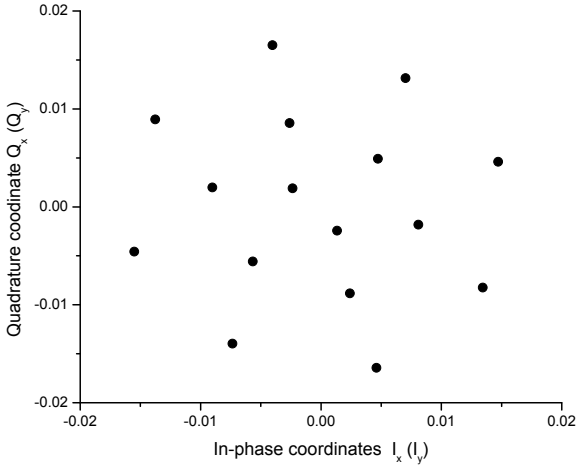

(b)

Figure 2.2 The optimized 2D 16-ary signal constellations: (a) For linear phase noise model, (b) For nonlinear phase noise model.

2.5 LDPC CODED MODULATION SCHEME

For convenience, we can use the likelihood function defined as [22],[38]

$$L(a_k, \theta_k) = \frac{p_R(r|a_k, \theta_k)}{p_R(r|a_k = 0)} \tag{2.13}$$

If the sequence of $L = T/T_s$ statistically independent symbols, $a = [a_1 \dots a_L]^T$, is transmitted, the corresponding likelihood function will be:

$$l(a, \theta) = \prod_{l=1}^{L} L(a_k, \theta_k) \tag{2.14}$$

To avoid numerical overflow problems, the log-likelihood function should be used instead, so we have that

$$l(a, \theta) = \log L(a, \theta) \tag{2.15}$$

Clearly, the ML approach leads to exponential increase in complexity as sequence length L increases. Here we propos a different strategy, which is inspired by Monte Carlo integration method. Namely, to calculate the log-likelihood function we will need to perform the following L -dimensional numerical integration:

$$l(a) = \log\left\{\int \dots \int \exp[l(a, \theta)]\, p_\Theta(\theta) d\theta\right\} \tag{2.16}$$

Instead of numerical integration, we propose to use Monte Carlo integration. Namely, by using the Monte Carlo integration, the log-likelihood function $l(a)$ can be estimated as:

$$l(a) = \log E_\theta\{\exp[l(a, \theta)]\} \tag{2.17}$$

where the expectation averaging E_θ is performed for different phase noise realizations. This method is particularly simple for memoryless phase noise processes, Wiener phase noise process and cyclic slip phase noise process described as a Markov process of reasonable memory. It can be shown that complexity of this method is $O\{(m^2 + L)N_r\}$, where m is the channel memory, L is the sequence length and N_r is the number of phase noise realizations. Compared to the ML method, whose complexity is $O\{M^L\}$, where M is the signal constellation size, complexity is significantly lower for long sequences to be detected. This method requires the knowledge of Markov phase noise process, which is quite easy to characterize by training. In particular, for the

Wiener phase noise process and memoryless phase noise process, the Gaussian noise generator is only needed. Also, we can also use the nonlinear phase noise model introduced in section 2.3 to generate the phase noise process [39].

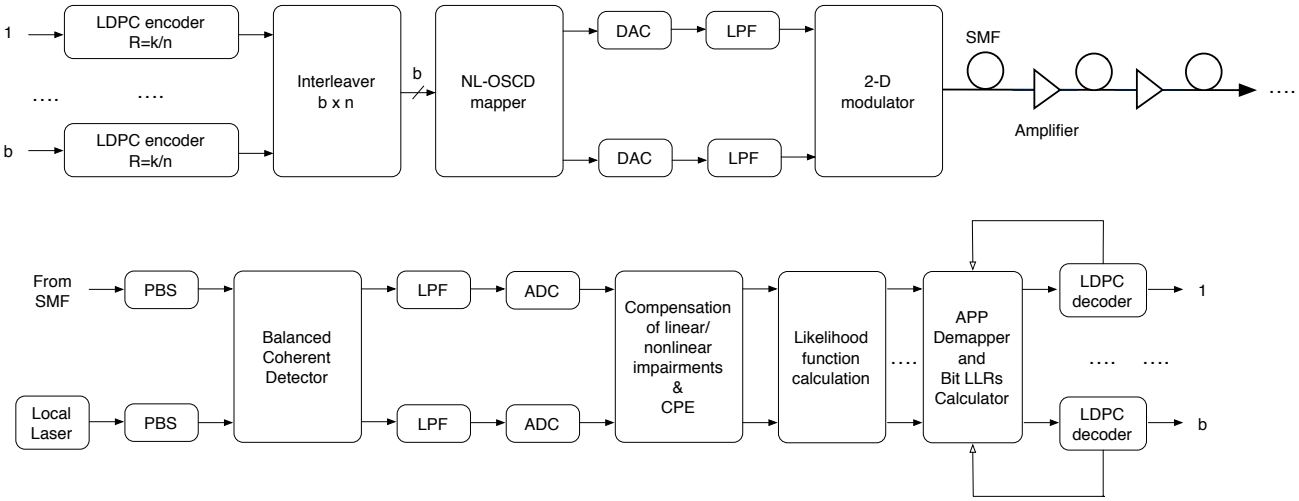

Figure 2.3 The LDPC coded modulation scheme with Monte Carlo integration to evaluate LLRs.

Our proposed LDPC coded modulation scheme we used in the simulation is shown in the Figure 2.3. The b independent data are first encoded by an (n, k) LDPC encoder and written in row-wise fashion into b×n block interleaver. Then either NL-OSCD or LLR-OSCD can be used for modulation and 2D (I/Q) modulator performs the electrical-to-optical conversion. Note that at the receiver side, we have implemented the Monte Carlo integration approach introduced above [40].

2.6 Performance Analysis

The LDPC coded modulation scheme intorduced in section 2.5 is used in simulation. The symbol rate is set to $R_s = 32.25$ GS/s and the quasi-cyclic LDPC (16935, 13550) code of rate 0.8 is used. All the results are obtained for 3 outer iterations and 20 inner (LDPC decoder) iterations.

2.6.1 Simulation for Linear Phase Noise Channel

The BER performance for LDPC-coded polarization-division multiplexed OSCD and LLR-OSCD constellation sets are summarized in the Figure 2.4. We have shown the performance different LLR-OSCD constellation sets optimized with different initial constellations (put in brackets) and different number of phase noise samples, denotes as *NS*. The constellation size is 16 and the frequency offset × symbol duration product is set to 10^{-3}. The green line denotes the BER performance of LLR-OSCD that uses the IPQ as initial constellation, while the black line is optimized from QAM. It is evident that the 16-ary LLR-OSCD optimized from QAM performs the best for 500 phase noise samples. The proposed LLR-OSCD with (*NS*=500) outperforms conventional QAM by 1.1 dB and OSCD by 0.2 dB.

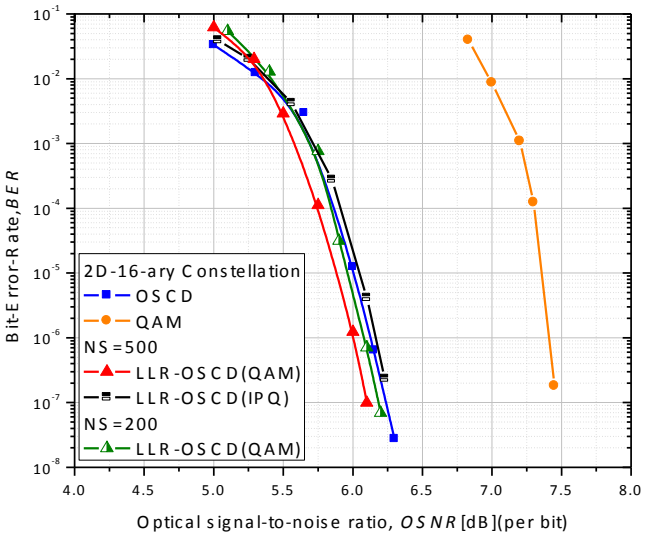

Figure 2.4 BER performance for proposed LLR-OSCDs.

2.6.2 Simulation for Nonlinear Phase Noise Channel

In simulations for nonlinear phase noise channel, we first fix the number of spans and the span length (the span length is 80km for all simulations), while vary the launch power in order to

determine the optimum launch power (minimizing the BER), as illustrated in Figure 2.5. The Figure 2.5 clearly indicates the existence of the optimal launch power for total transmission distance of 4000 km for both 8-ary NL-OSCD and 8-QAM. It can also be noticed that the nonlinear tolerance of 8-NL-OSCD is better. NL-OSCD (1, 2000) curve denotes that this constellation has been obtained by employing the algorithm described in Sec. 3 with the launch power of 1 dBm and total transmission distance of 2000 km. We can see that NL-OSCDs with different parameters have similar optimal power around 1 dBm. Then we fix the span length and launch power in order to see the performance of difference constellations with total transmission length. The total transmission distance that can be achieved by employing NL-OSCDs and LDPC coding is around 6700 km, as shown in Figure 2.5.

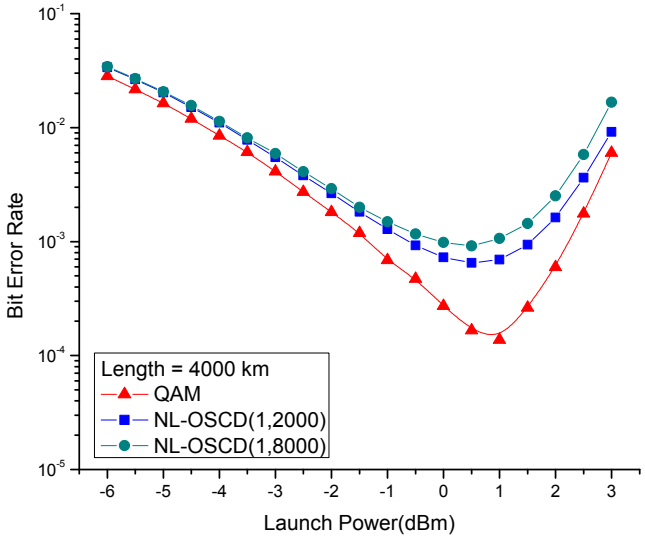

Figure 2.5 Uncoded BER vs. launch power for 8-ary NL-OSCD and QAM.

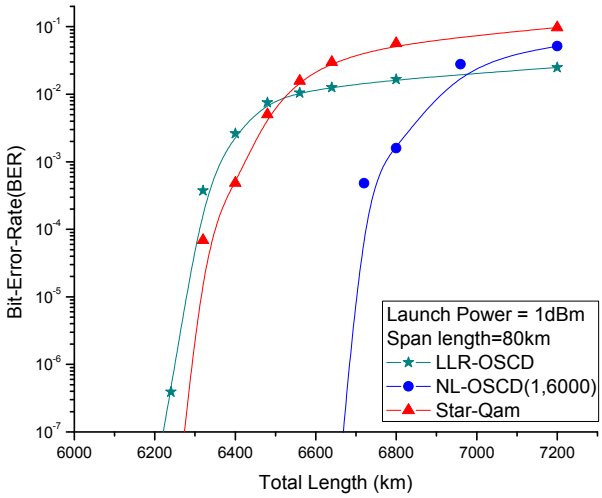

Figure 2.6 Coded BER vs transmission length plot for 8-ary NL-OSCD and QAM.

In Figure 2.6, we use LLR-OSCD to denote the constellation designed for linear phase noise dominated scenario. It is obvious to see that the NL-OSCD outperforms 8-ary star-QAM for almost 500 km. Notice that LLR-OSCD performs a little worse than the QAM, which indicates that LLR-OSCD is not suitable for the channel model. We then perform the similar study for 16-ary-NL-OSCD and the results are summarized in Figure 2.7 and Figure 2.8.

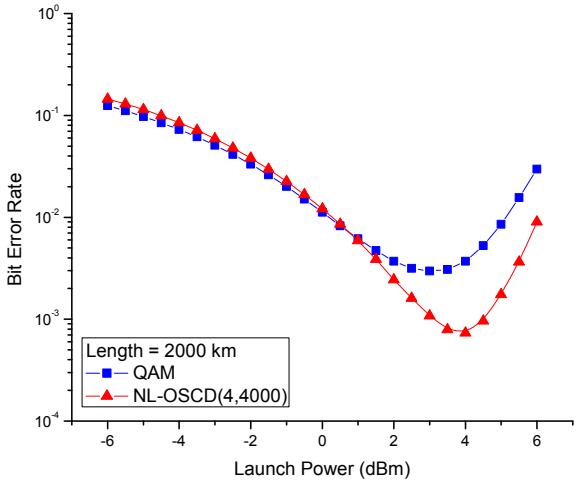

Figure 2.7 Uncoded BER vs. launch power for 16-ary NL-OSCD and QAM.

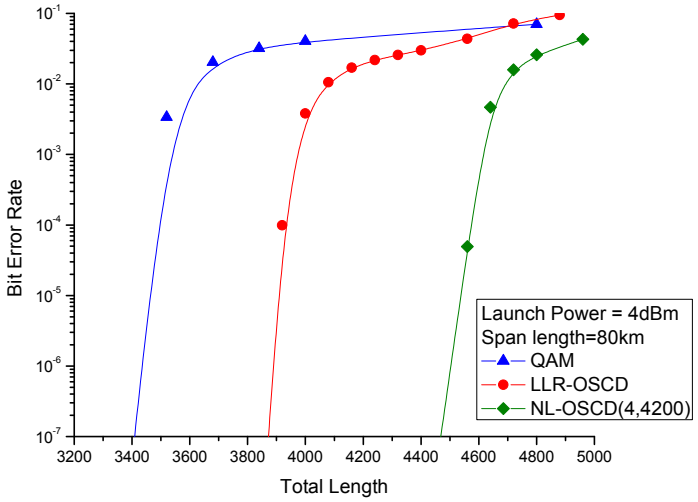

Figure 2.8 Coded BER vs transmission length plot for 16-ary NL-OSCD and QAM.

The optimal power for 16-ary NL-OSCD is 4 dBm, as shown in Figure 2.7, and the total transmission distance exceeds 4400 km, as shown in Figure 2.8. The transmission distance can be further increased by employing the turbo equalization principle, which is out of scope of this dissertation. The Figure 2.7 indicates that 16-ary NL-OSCD has better nonlinear tolerance than 16-QAM. On the other hand, Figure 2.8 indicates that the 16-ary NL-OSCD outperforms 16-QAM by almost 1000 km and LLR-OSCD by 600 km. The new signal constellations obtained by using the proposed algorithm clearly have better nonlinear tolerance and can significantly extend the total transmission distance of QAM. The reason is that we take the nonlinear nature of the channel into consideration when designing the constellation.

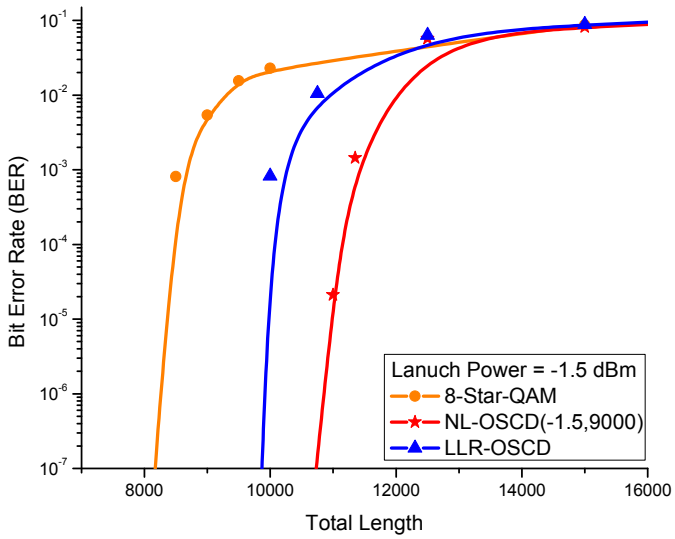

Figure 2.9 BER vs transmission length plot for 16-ary NL-OSCD and QAM.

In Figure 2.9, we provide some interesting result in the simulation. If we increase the span length to 100 km. The total transmission length of 8 ary-NL-OSCD can achieve almost 11000 km with launch power of -1.5 dB. Also, it still performs better than QAM as well as LLR-OSCD significantly.

2.7 MULTIDIMENSIONAL OSCD FOR SPM

The 4-dimensional (4D) signal constellation can be directly used in optical transmission with the use of polarization multiplexing. Polarization switched quadrature phase-shift keying (PS-QPSK) has been studied in [41] and can be considered as 8-ary 4D constellation sets, which is the conventional modulation format used in polarization multiplexing transmission. Meanwhile, some other constellation design algorithms such as sphere-packing (SP) algorithm [42] have been proposed. However, rare of these algorithms has taken the fiber nonlinearities into account. The fiber nonlinearities is one of the most important factors in the limitation of coherent long-haul optical transmission system [43]. When optical signal is transmitted through an optically

amplified fiber optical communication link, the nonlinear phase noise introduced by Kerr nonlinear effects, in addition to nonlinear signal-to-ASE noise interaction, will accumulate every span. In this section, we propose the new multidimensional signal constellation design algorithm, which is applicable to coherent detection systems in the presence of nonlinear phase noise.

As an extension of the optimum signal constellation algorithm (OSCD), which is introduced in [2], the proposed algorithm, named as multidimensional nonlinear optimal signal constellation design (ND-NL-OSCD), has been expended to multidimensional space and uses the cumulative log-likelihood function instead of the Euclidian distance as criterion of optimization. Meanwhile, a LDPC coded modulation scheme suitable for use of the multidimensional constellation sets obtained from the proposed algorithm has also been proposed. The Monte Carlo simulation shows that our proposed signal constellation sets significantly outperforms PS-QPSK and Sphere Packing constellations.

2.7.1 The OSCD for SPM dominated channel

The multidimensional signal constellation design is different with the conventional OSCD algorithm proposed in [18]. With the use of polarization multiplexing, there are two scenario will be considered. Let the size of constellation be M and $S = \log_2 M$ is the number of bits per symbol. If the PMD can be compensated perfectly or has little effect and can be ignored, two polarizations can be considered as two independent channels. In this case, we can directly use $2^{S/2}$-ary 2D-NL-OSCD constellation [44] for each polarization resulting in M-ary 4D-NL-OSCD constellations if S can be divided by 2, which can be considered as generating 4D constellations with cartesian product of 2D constellations. However, this cartesian product method cannot generate 4D constellations if S cannot be divided by 2 and becomes inaccurate if PMD cannot be totally compensated. In these cases, we will use multidimensional optimal signal constellation

design algorithm instead of inner production method to generate 4D signal constellations. In this dissertation, we will consider the 8-ary and 32-ary 4D-NL-OSCD generated by the algorithm and 16-ary 4D-NL-OSCD generated by inner product of 4-ary 2D-NL-OSCD as our optimized signal constellation.

The multidimensional optimal signal constellation design algorithm is similar to OSCD algorithm [2] but now expanding to multidimensional case. Meanwhile, by changing the optimization criterion to maximizing the cumulative log-likelihood function, we can make the resulting constellation suitable for nonlinear phase noise dominated channel. The optimum source distribution for the nonlinear phase noise channel can be obtained by Arimoto-Blahut algorithm and we can generate the training samples from this source. Then we run our proposed algorithm, which is described below. In this algorithm, we perform clustering of the constellation points generated by optimum source based on cumulative log-likelihood function. New constellation points will be then obtained by calculating the center of mass of such obtained clusters. This procedure is repeated until convergence or until a predetermined number of iterations has been reached.

The proposed multidimensional nonlinear optimum signal constellation design (ND-NL-OSCD), can be formulated as follows.

1) Initialization: Choose the signal constellation that will be used for initialization and normalize the power of constellation to target launch power P. (Both ND-SP and cartestian product QAM constellation can be used as initialization.) Let the size of constellation be M.
2) Generate the training sequence from the optimum source distribution. Denote this sequence as $\{x_j;\ j = 0, \ldots, n-1\}$.

3) The clustering step. Group the samples from this sequence into M clusters. The membership to the cluster is determined based on the log-likelihood ratio (LLR) of sample point and candidate signal constellation points from previous iteration. Each sample point is assigned to the cluster with the largest LLR. Given the m th subset (cluster) with N candidate constellation points, denoted as $\widehat{A}_m = \{y_i\ ;\ i = 1, \dots, N\}$, find the log-likelihood (LL) function of partition $P(\widehat{A}_m) = \{S_i\ ;\ i = 1, \dots, N\}$ as follows

$$LL_m = LL\left(\left\{\widehat{A}_m, P\left(\widehat{A}_m\right)\right\}\right) = n^{-1}\sum_{k=0}^{n-1}\max_{y\in\widehat{A}_m} LL(x_k, y) \tag{2.18}$$

The function $LL(x_j, y)$ is the cumulative log-likelihood function defined as

$$\begin{aligned} LL(x_k, y) = \frac{1}{NS}\sum_{i=1}^{NS} -\{ & \frac{\left\{x_{k1} - Re\left[(y_1 + y_2 j)e^{-j\times PN_{i,1}}\right]\right\}^2}{2\delta^2} \\ & + \frac{\left\{x_{k2} - Im\left[(y_1 + y_2 j)e^{-j\times PN_{i,1}}\right]\right\}^2}{2\delta^2} \\ & + \frac{\left\{x_{k3} - Im\left[(y_3 + y_4 j)e^{-j\times PN_{i,2}}\right]\right\}^2}{2\delta^2} \\ & + \frac{\left\{x_{k4} - Im\left[(y_3 + y_4 j)e^{-j\times PN_{i,2}}\right]\right\}^2}{2\delta^2}\} \end{aligned} \tag{2.19}$$

where NS denotes the number of phase noise samples and the corresponding nonlinear phase noise sample from X and Y polarizations are denoted as $PN_{i,1}$ and $PN_{i,2}$, which can be generated using the channel model described in Section 2. $x_{k1}, x_{k2}, x_{k3}, x_{k4}$ denote the coordinates of the constellation point x_k. Similarly, y_1, y_2, y_3, y_4 denote the coordinates of the received vector (point) y.

4) Determine the new signal constellation points as the center of mass for each cluster.

Repeat the steps 2)-3) until convergence.

As an illustration, in Figure 2.10 (a), we provide the result of our proposed algorithm for 4D 8-ary NL-OSCD, which is optimized at launch power of -4 dBm and transmission length of 9600km. Meanwhile, we also show the PS-QPSK as an comparison in Figure 2.11(b). The red points and blue points denote the constellations at X and Y polarization. The point with same number index indicates the transmission pair at same time slot. That is to say, the points on X and Y polarizations with same number will be transmitted at the same symbol duration. It is obvious that our proposed NL-OSCD has split the center points to a small QPSK (the 5,6,7,8 points on X-polarization and 1,2,3,4 on Y-polarization) while the PS-QPSK remains same one point.

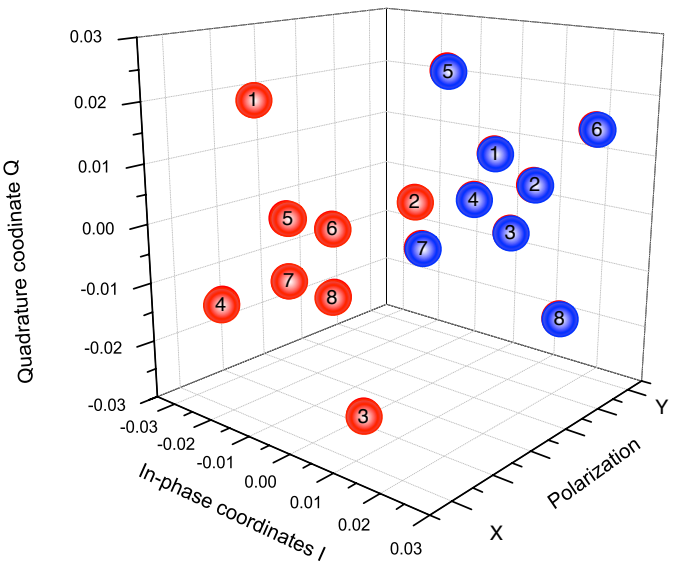

(a)

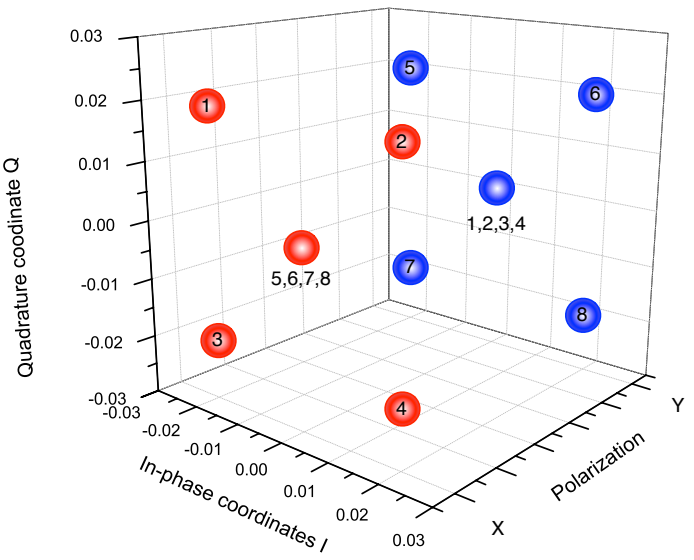

(b)

Figure 2.10 An illustration of 4D 8-ary signal constellations: (a) The optimized 8-ary 4D-NL-OSCD Constellation. (b) The PS-QPSK.

For 16-ary 4D signal constellation design, we can directly use the cartesian product of 4-ary 2D-NL-OSCD because we do not consider PMD in our model and $S = 4$ can be divided by 2. Note that it has been proved that 4-ary 2D-NL-OSCD is same as QPSK. So the resulting 16-ary 4D signal constellation is also same as polarization multiplexing QPSK (PM-QPSK). That is to say, PM-QPSK is the optimal 16-ary 4D constellations for nonlinear phase error dominated channel and without consideration of PMD. Similarly, for 32-ary 4D signal constellation design, we will directly use our proposed algorithm because $S = 5$ cannot be divided by 2.

2.7.2 The LDPC coded modulation scheme

Our proposed LDPC coded modulation scheme we used in the simulation is shown in the Figure 2.11. The b independent data are first encoded by an (n, k) LDPC encoder and written in row-

wise fashion into b×n block interleaver. Then 4D-NL-OSCDs have been used for modulation. The first two coordinates of the constellation are modulated onto X-polarization and last two coordinates are modulated onto Y-polarization. Note that at the receiver side, we have implemented the Monte Carlo integration approach, introduced in [35], in order to estimate the log-likelihood function:

$$l(a) = \log E_{\Phi_{NL}}\{\exp\,[l(a, \Phi_{NL})]\} \tag{2.20}$$

where $l(a, \Phi_{NL})$ is the log-likelihood function for the transmitted symbols and $E_{\Phi_{NL}}$ is the expectation average over the nonlinear phase Φ_{NL}. Based on Equation (2.20), the log-likelihood can be calculated after the coherent detection and carrier phase estimation (CPE). The LDPC decoders perform decoding for b data streams at the same time and the extrinsic information is iterated between APP demapper and LDPC decoders.

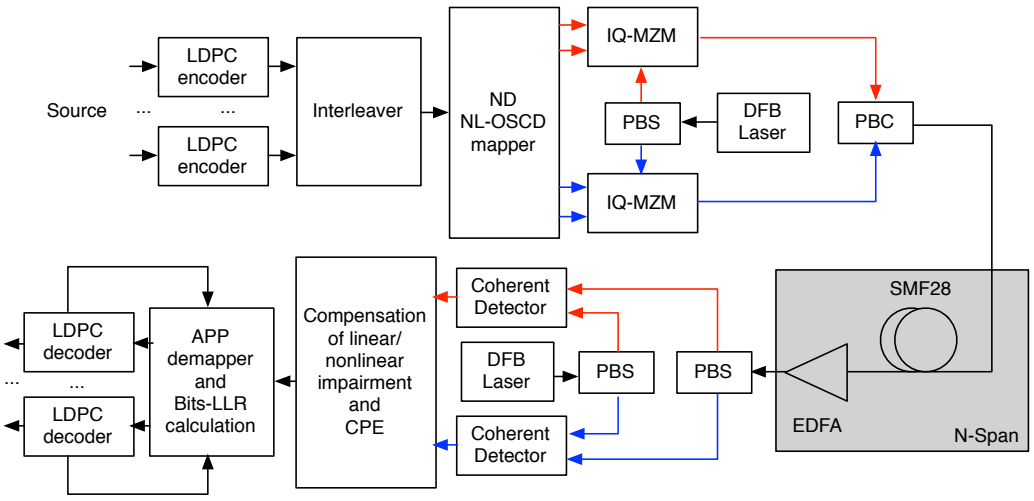

Figure 2.11 The LDPC coded modulation scheme with Monte Carlo integration to evaluate LLRs.

2.7.3 Numerical Result

In the simulation, the symbol rate is set to $R_s = 32.25$ GS/s and the quasi-cyclic LDPC (16935, 13550) code of rate 0.8 is used. All the results are obtained for 3 outer iterations and 20 inner

(LDPC decoder) iterations. The span length has been fixed to 80km. Notice that ND-NL-OSCD is dependent on the launch power and transmission length but the shape of ND-NL-OSCD does not change too much for different powers and lengths. So it is possible to define a typical ND-NL-OSCD, which can be then optimized at launch power of -4 dBm and distance of 9600 km for 8-ary 4D constellation size. For 32-ary 4D constellation the launch power is -7dBm and transmission length is 7200 km. These parameters are chosen by analysis of the optimal power and transmission length.

In simulations, we first fix the transmission length and vary the launch power in order to find the optimal power, which is shown in Figure 2.12. It is obvious that for 8-ary 4D-NL-OSCD, the optimal power is -4dBm. For PS-QPSK and 8-ary 4D sphere packing (SP) constellation, the optimal power is -6dBm. Meanwhile, we can see that our proposed 4D-NL-OSCD has better BER performance comparing to other two constellation sets. We will further prove these observations with the analysis of Figure 2.13.

In Figure 2.13, we fix the launch power to the optimal power of each constellation set and find relation between BER and transmission length. It is obvious that our proposed 8-ary 4D NL-OSCD outperforms PS-QPSK and 8-ary 4D SP constellation. Meanwhile, the situation is same for 32-ary case. Because the 16-ary 4D-NL-OSCD is same as PM-QPSK, we can also see that PM-QPSK outperforms 16-ary 4D SP constellation.

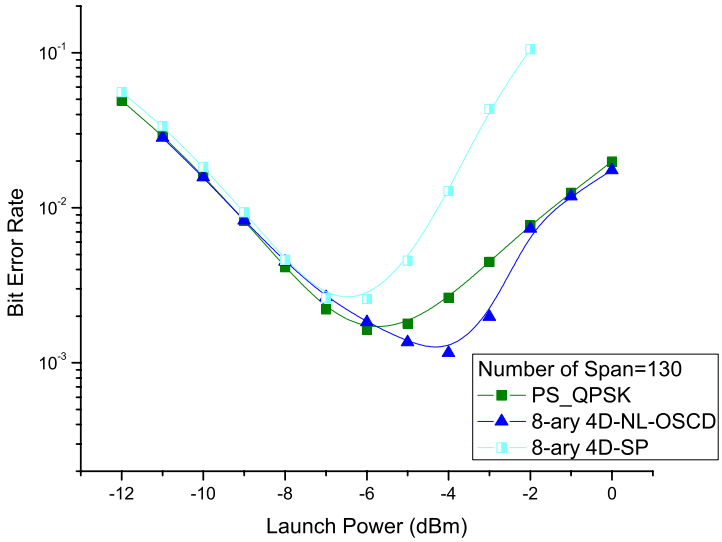

Figure 2.12 The BER vs Launch Power curves for 8-ary 4D constellation sets.

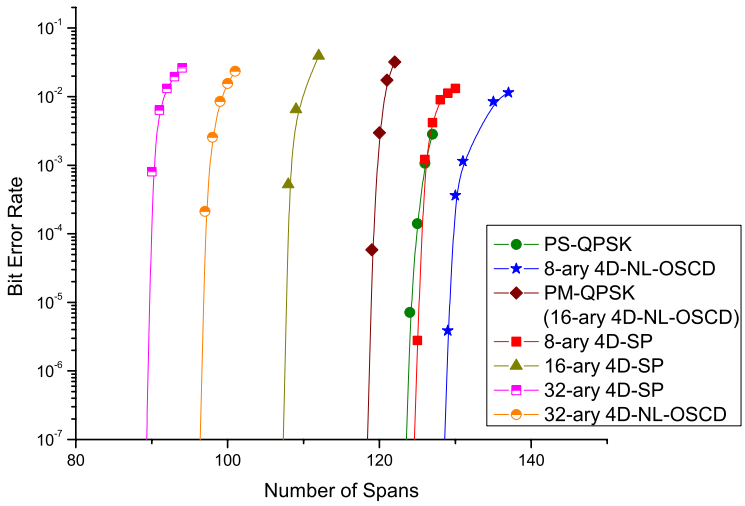

Figure 2.13 The BER vs Transmission Length curves for 4D constellation sets.

In this section, we proposed a new multidimensional signal constellation, which is suitable for coherent optical channels dominated by the nonlinear phase noise. The constellation design process can either be directly using algorithm or inner production of corresponding 2D

constellations based on different scenario. By using log-likelihood function as the design criterion instead of the Euclidean distance, we can take the nonlinear nature of the channel into account. The Monte Carlo simulations demonstrate that for 8-ary 4D NL-OSCDs outperform the corresponding PS-QPSK constellations for almost 400 km. For 16-ary and 32-ary, our proposed constellation sets outperforms sphere-packing constellation by 800 and 640 km.

2.8 CONCLUSION

In this chapter, our goal was designing the signal constellation sets that are more tolerant to linear or nonlinear phase errors. [45] We combine the OSCD with both linear and nonlinear phase error estimator based on proposed channel model, which can be used to design signal constellations suitable for coherent optical channels dominated by either linear or nonlinear phase noise channel. By using log-likelihood function as the design criterion instead of the Euclidean distance, we can take the nonlinear nature of the channel into account. Meanwhile, we have expanded this algorithm to multidimensional case. The Monte Carlo simulations demonstrate that for 8-ary and 16-ary cases, NL-OSCDs outperform the corresponding QAM constellations for almost 500 km and 1000 km. The LLR-OSCD outperforms QAM constellation by 1.1 dB for 8-ary constellation.

CHAPTER 3

SIGNAL CONSTELLATION DEISGN FOR CROSS PHASE MODULATION DOMINATED CHANNEL

3.1 INTRODUCTION

Wavelength-division-multiplexed (WDM) systems have been extensively studied in currently existing literature [46]-[47]. As the launch power increases, the nonlinear signal and noise interaction becomes relevant, and in WDM systems the nonlinear interaction between WDM channels is an important factor in performance degradation. For optical fibers with nonzero chromatic dispersion coefficient, the interchannel nonlinearities between WDM channels are typically due to cross-phase modulation (XPM) arising from the Kerr effect. Different approaches to signal constellation design have been investigated in order to deal with degradation caused by nonlinearities. Given the complexity of the problem, typically the signal constellation design for the self-phase modulation (SPM) dominated scenario has been studied [31],[48],[49]. Unfortunately, not many researches have focused on the signal constellation design for the XPM dominated channel, which is the subject of this chapter.

In this chapter, we first describe a channel model suitable for study of coherent detection WDM systems dominated by the residual nonlinear phase noise introduced by XPM, then a new signal constellation design, obtained by generalization of [2], but now applicable to XPM dominated channel, is also proposed. We define the cumulative log-likelihood function and use it as an optimization criterion instead of using the Euclidian distance as optimization criterion used in [2], which is optimum only for additive white Gaussian noise (AWGN) channel and has been verified by experiments [51]-[52] and section 1.6. The optimum source distribution is obtained by maximizing the mutual information, based on the Arimoto-Blahut algorithm [4]. Since the proposed signal constellation design algorithm is optimum for the XPM dominated channel, it has been named here as XPM-based optimum signal constellation design (XPM-OSCD) algorithm. Moreover, a collaborative demodulation scheme suitable for WDM systems

employing XPM-OSCD constellation is also proposed in this paper. Monte Carlo simulations indicate that the WDM lightwave system based on XPM-OSCD significantly outperforms the corresponding LDPC-coded QAM by increasing the transmission length by 600 km. We demonstrate by simulations that the proposed demodulation scheme further increases the transmission length by more than 2000km for 16-ary constellation.

3.2 THE CROSS PHASE MODULATION DOMINATED CHANNEL MODEL

The XPM-induced channel impairments have been intensively studied in optical fiber transmission, such as in [53]. There are several theoretical XPM dominated channel models, which were verified by both simulations and experiments [54]-[57]. Our channel model is targeting the worst-case scenario, and it is based on the pump-probe model with discrete amplification for the finite number of fiber spans. Meanwhile, the purpose of this channel model is to explore the signal constellation design method for the XPM dominated channels and to analyze how much improvement we can get by only optimizing the signal constellation sets. When the optical signal is periodically amplified by EDFAs, the phase error is unavoidably added to the optical signal, which can be simulated by the pump-probe model, and accumulated as the number spans increases. For convenience, we consider the discrete memoryless channel model, which is introduced in [31] and can be described as follows:

$$Y = (X + Z)e^{-j\Phi_{XPM}} \tag{3.1}$$

where $X \in \mathcal{X}$ is the channel input, Z is the total additive noise, and Y is the channel observation. (In (3.1) j denotes the imaginary unit.) For single channel transmission, in each fiber span of length L, the self-phase modulation phase shift Φ_{SPM} is given by

$$\Phi_{SPM} = \int_0^L \gamma P(z)dz = \gamma L_{eff} P \tag{3.2}$$

where P is the launch power and γ is the nonlinear Kerr-parameter. For a fiber span length of L with attenuation coefficient of α, the power evolution is described as $P(z) = Pe^{-\alpha L}$ and the effective length is defined as

$$L_{eff} = \frac{1 - e^{-\alpha L}}{\alpha} \tag{3.3}$$

On the other hand, in WDM systems, for N_A fiber spans, the overall nonlinear phase noise due to XPM is given by:

$$\Phi_{XPM} = \gamma L_{eff} \left\{ \sum_{k=0}^{2} \sum_{i=1}^{N_A} \left| E_k + \sum_{j=1}^{i} n_j^k \right|^2 \right\} \tag{3.4}$$

where E_0, E_1 and E_2 denote the transmitted electric field of the observed wavelength channel and its two neighboring WDM channels, n_j^k denotes the additive noise at the jth span in the kth channel, which is independent identically distributed zero-mean circular Gaussian random complex variable with variance δ_k^2. The total additive noise for each channel at the end of all fiber segments has the variance $\delta_{total\_k}^2 \triangleq E[Z^2] = 2N_A\delta_k^2$ and can be calculated as [18]: $\delta_{total\_k}^2 = 2n_{sp}h\nu\alpha\Delta\nu N_A L$. The introduced channel model can be considered as the worst-case scenario of XPM dominated WDM channel with the signal spacing close to symbol rate.

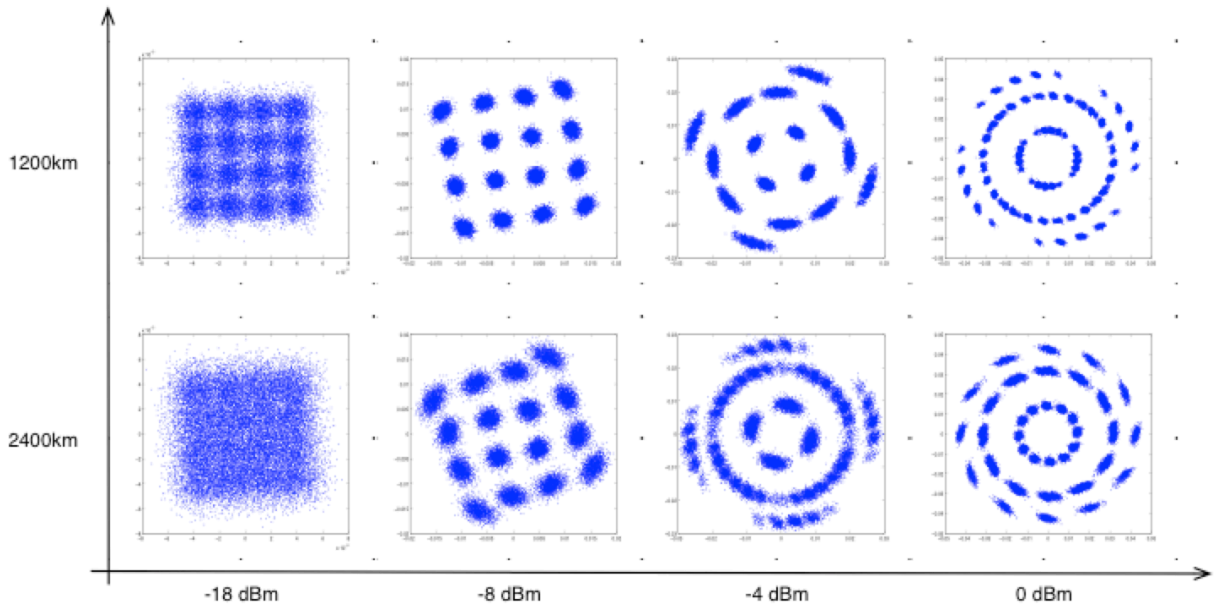

Figure 3.1 Received signal constellations for different transmission lengths and launch powers.

In this channel model, the variance of the phase error is dependent on the channel input and the channel is decided by the number of spans, transmission length, and also by the launch power. In our case, the span length is set to 80 km, and then we first fix the transmission length to find the optimal launch power and compare the BER versus transmission distance curve based on the optimal power. The parameters used in the simulation are summarized in Table 2.1, while an illustration of the received symbols for different transmission lengths and launch powers is shown in Figure 3.1. It is evident that the XPM effects become more relevant as the transmission length and/or launch power increase.

3.3 Signal Constellation Sets for XPM Dominated WDM System

For XPM dominated WDM system, we can use an algorithm similar to OSCD algorithm [19] but now changing the optimization criterion from minimizing the mean square error to maximizing

the cumulative log-likelihood function in order to make the constellation suitable for XPM dominated channel. The optimum source distribution for the nonlinear phase noise channel can be obtained by Arimoto-Blahut algorithm and then we can generate the training samples from this source. In this algorithm, we perform clustering of the constellation points generated by optimum source based on cumulative log-likelihood function. New constellation points will be then obtained by calculating the center of mass of such obtained clusters. This procedure is repeated until convergence or until a predetermined number of iterations has been reached. The cumulative log-likelihood function $\mathrm{LL}(x_j, y)$, used in optimization, is defined as

$$\mathrm{LL}(x_k, y) = \frac{1}{NS}\sum_{i=1}^{NS} -\frac{\left\{x_{k1} - \mathrm{Re}\left[(y_1 + y_2 j)e^{-j\times PN_i}\right]\right\}^2 + \left\{x_{k2} - \mathrm{Im}\left[(y_1 + y_2 j)e^{-j\times PN_i}\right]\right\}^2}{2\delta^2} \tag{3.5}$$

where NS denotes the number of phase error samples and the corresponding nonlinear phase error sample is denoted as PN_i, which can be generated using the channel model described in Section 3.2 (see equation (3.4)). When increasing or decreasing the number of WDM channels in the target scheme, the level of noise samples will also change, which will make the algorithm always suitable for any target scheme. Meanwhile, the algorithm should be repeated for different WDM channels under consideration as every channel might experience a different XPM effects. x_{k1} and x_{k2} denote the first and second coordinates of the constellation point x_k. Similarly, y_1 and y_2 denote the coordinates of the received vector (point) y. The equation above is applicable to two-dimensional (2D) signal constellation designs, but it can straightforwardly be generalized for arbitrary dimensionality.

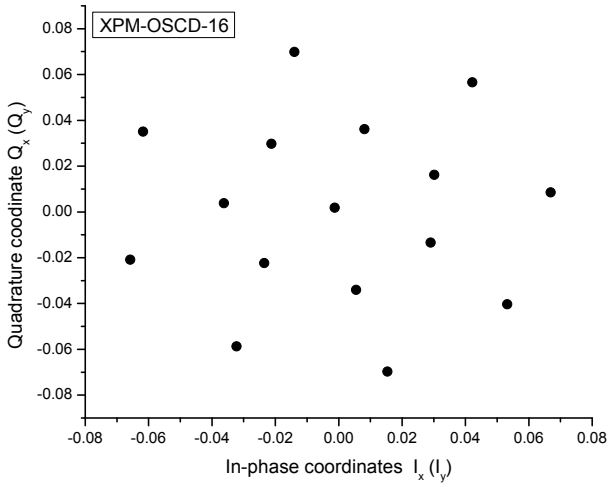

Figure 3.2 The 16-ary XPM-OSCD constellation.

As an illustration, in Figure 3.2 we provide our resulting 16-ary XPM-OSCD constellation, which is obtained for XPM dominated scenario in the presence of ASE noise, optimized at launch power of 1 dBm and transmission distance of 2720 km.

3.4 COLLABORATIVE DEMODULATION SCHEME FOR XPM DOMINATED WDM SYSTEMS

Our proposed LDPC coded modulation scheme, suitable for WDM systems with polarization-division multiplexing, we used in the simulation, is shown in the Figure 3.3(a). (To facilitate explanations only single polarization state is shown.) For each WDM channel, the b independent data streams are first encoded by the (n, k) LDPC encoders, whose codewords are written in row-wise fashion into $b \times n$ block-interleaver. Then XPM-OSCDs have been used for modulation and 2D (I/Q) modulator performs the electrical-to-optical conversion. The LDPC decoders perform decoding of b data streams at the same time and the extrinsic information is iterated

between the a posteriori probability (APP) demapper and LDPC decoders. This system can straightforwardly be generalized to the multi-dimensional case. Note that at the receiver side, we have implemented the Monte Carlo integration approach, introduced in [19], in order to estimate the log-likelihood function of transmitted sequence a:

$$l(a) = \log E_{\Phi_{XPM}}\{\exp\,[l(a, \Phi_{XPM})]\} \tag{3.6}$$

where $l(a, \Phi_{XPM})$ is the log-likelihood function for the transmitted symbols in the presence of XPM and $E_{\Phi_{XPM}}$ is the expectation average over the nonlinear phase introduced by XPM. Based on equation 3.6, the log-likelihood can be calculated after the carrier phase estimation (CPE).

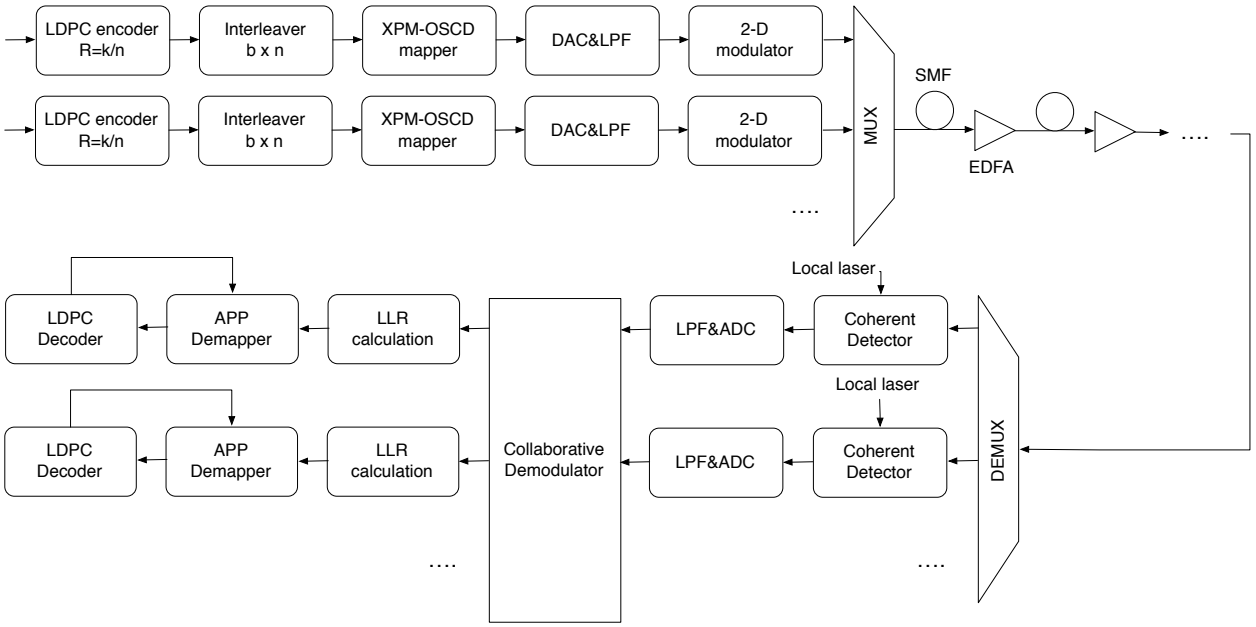

(a)

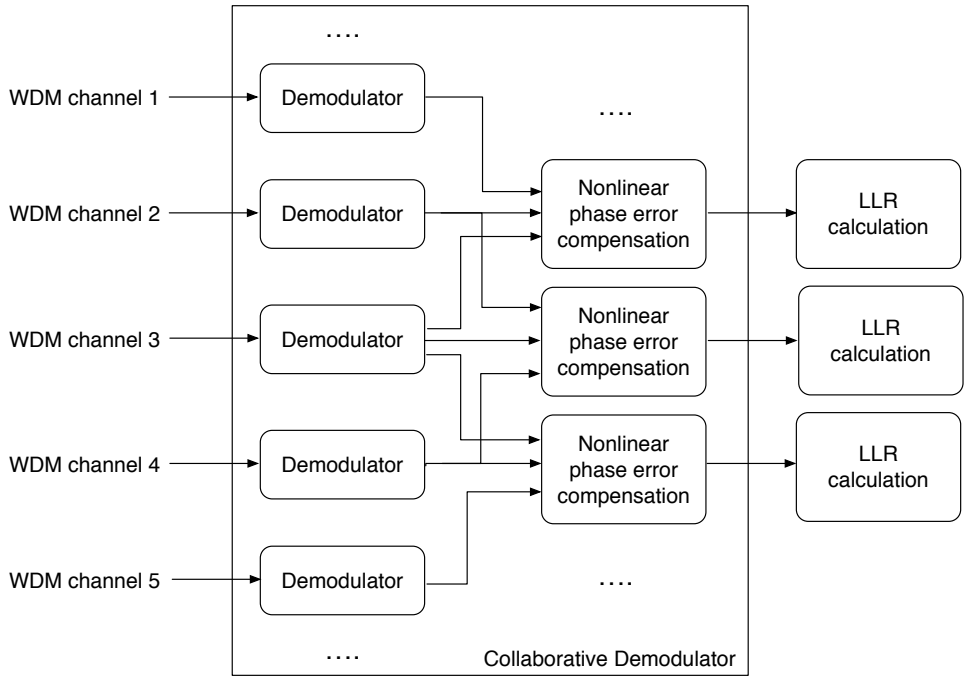

(b)

Figure 3.3 (a) Collaborative LDPC coded WDM transmission scheme. (Only single polarization is shown to facilitate the explanations.) (b) Details of the collaborative demodulation (CDM) scheme.

In order to get accurate phase error estimation, we propose a collaborative demodulation (CDM) scheme, with details shown in Figure 3.3(b). The received signal is first passed to the demodulator, whose output is one of the constellation points with the minimum distance to the received symbol. Then this output will be sent to the nearby channels. With all three outputs available, including one from target channel itself, the phase estimator will perform the propagation using the channel model introduced in Section 3.2 and generate an estimation of the phase error, which will be used as Φ_{XPM} in equation (3.6). This process can be considered as a digital back propagation on a XPM channel model of low complexity. We first estimate the XPM introduced the nonlinear phase noise by employing the channel model introduced in Section 3.2,

followed by the Monte Carlo integration approach to estimate the log-likelihood function of transmitted sequence. The estimation of XPM introduced nonlinear phase noise is performed by our proposed collaboration demodulation scheme, which takes the nonlinear phase noise from neighboring WDM channels into account. The demodulator also sends the original received symbols to LLR calculation block for the target channel.

3.5 NUMERICAL RESULTS

The simulation results for LDPC coded WDM transmission based on XPM-OSCD constellations are summarized in Figure 3.4 and 3.5. The scheme is based on 3-channel DWDM. The symbol rate is set to $R_s = 32.25\ \mathrm{GS/s}$ and the quasi-cyclic LDPC (16935, 13550) code of rate 0.8 is used. All the results are obtained for 3 outer iterations and 20 inner (LDPC decoder) iterations. For 8-ary OSCD-XPM simulations, the nearby channels all use 8-QAM as modulation format. With PDM and when two orthogonal subcarriers are used, each WDM channel is compatible with 400 Gb/s per WDM channel transmission. In simulations, we first fix the transmission length, which is chosen as the largest error-free transmission length possible at coded case, while varying the launch power in order to determine the optimum launch power (in minimizing the BER sense). The Figure 3.4 clearly indicates that the optimal launch power for 8-ary XPM-OSCD is about -10 dBm. It can also be noticed that the XPM tolerance of 8-XPM-OSCD is better. Meanwhile, the gap between QAM and XPM-OSCD has become larger when applying the CDM technique, compared to the case when CDM is not used. On the other hand, when the XPM effect is too strong or not compensated for at the receiver side, the improvement brought by XPM-OSCD is smaller. We can also see the optimal launch power for the system with collaborative demodulation scheme is about -5 dBm.

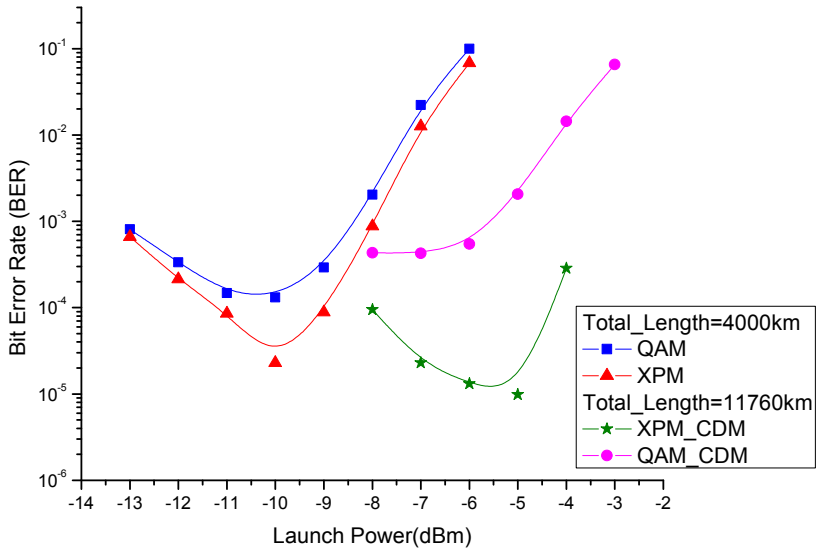

Figure 3.4 Uncoded BERs vs launch power for 8-ary signal constellations.

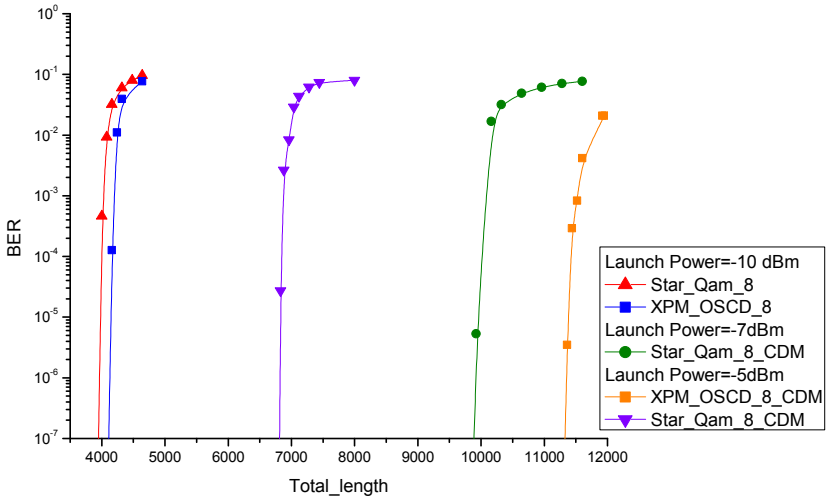

Figure 3.5 LDPC-coded BERs vs total transmission distance for 8-ary signal constellations.

In Figure 3.5, we show the result for 8-ary XPM-OSCD constellations as well as 8-QAM provided for comparison purpose. Additionally, the BER performance vs. total transmission distance with or without collaborative demodulation is also shown in the figure. The "CDM"

notation is used to denote the WDM system equipped with collaborative demodulation scheme, as indicated above. It is clear to see that the XPM-OSCD constellations perform better than 8-QAM about 240 km without collaborative demodulation scheme. For the system with the collaborative demodulation scheme, the XPM-OSCD outperforms 8-QAM for about 1500 km with each systems operating at their optimal power. If operating at the same power (-5 dBm), the XPM-OSCD outperforms 8-QAM for about 3000 km.

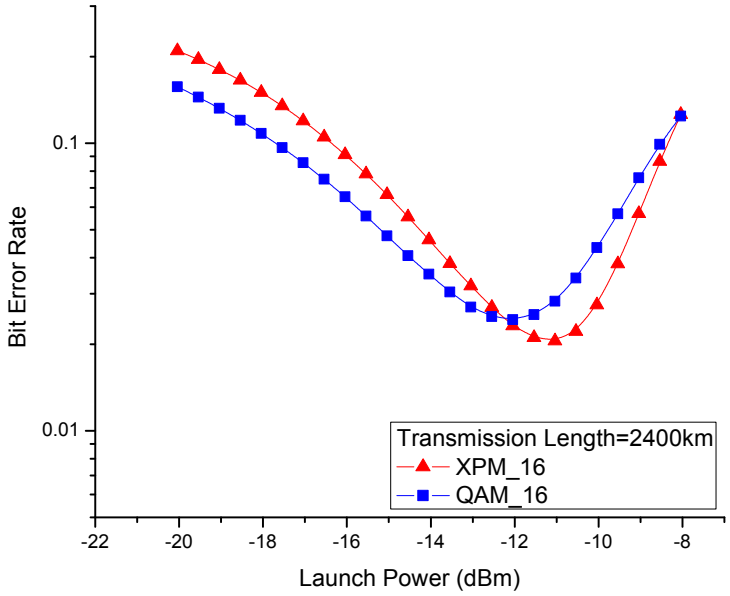

Figure 3.6 Uncoded BERs vs launch power for 16-ary constellations.

In Figure 3.6 and Figure 3.7, we show the corresponding results for 16-ary XPM-OSCD constellations. Note that the optimal power for the WDM system based on 16-ary constellations is about -11dBm. It is clear to see that the XPM constellation outperforms 16-QAM more than 600km when the collaborative demodulation scheme is not used. It is evident that our proposed collaborative demodulation scheme can further extend the transmission length by even 2000 km.

When the CDM scheme is also applied for 16-QAM, at this scenario, XPM constellation still performs better than QAM for about 600km.

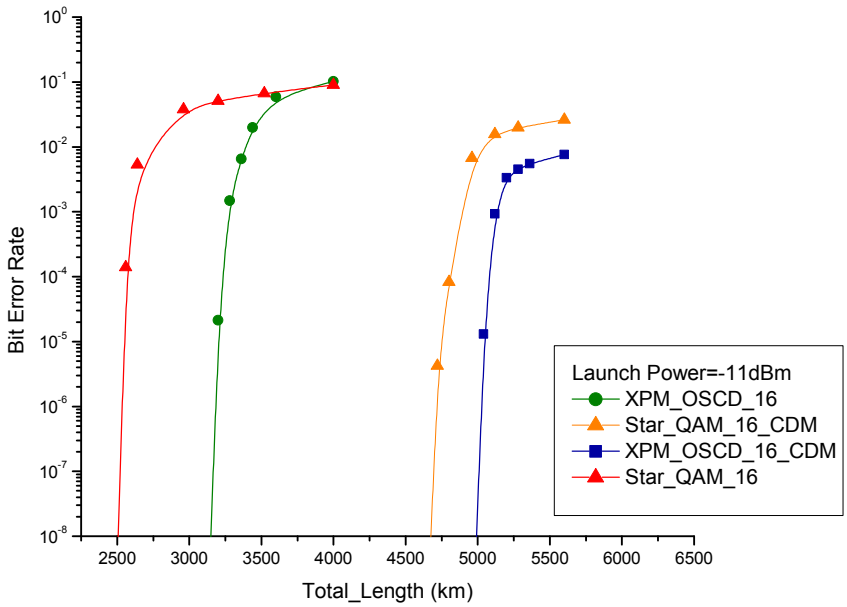

Figure 3.7 LDPC-coded BERs vs total transmission distance for 16-ary constellations.

3.6 CONCLUSION

In conclusion, we have proposed the signal constellation design algorithm suitable for XPM dominated WDM channels. Additionally, the collaborative demodulation scheme has been proposed, compensating for the nonlinear phase noise due to XPM. The proposed signal constellation design algorithm employs the log-likelihood function as the optimization criterion. The Monte Carlo simulation shows that both 8-ary and 16-ary constellations obtained by XPM–OSCD algorithm outperform corresponding QAM constellations, when non-collaborative demodulation scheme is used. On the other hand, when proposed collaborative demodulation scheme has been used the transmission length can be extended significantly.

CHAPTER 4

NON-UNIFORM SIGNALING BASED CODED MODULATION SCHEME

4.1 INTRODUCTION

In order to achieve high data rate and spectral efficiency in optical communications, high-order and multi-dimensional modulation formats are proposed [60][61]. In the conventional data transmission schemes, the probability of each point in a given constellation is transmitted equally likely and the constellation sets are set to 2^n. However, this scheme does not take into account the different energy cost of various constellation points. The idea of choosing constellation points with a non-uniform probability distribution is explored in previous studies [62][63], but not in optical communication context. Such non-uniform signaling will reduce the entropy as well as the transmitter output. However, if the points with low energy are transmitted more often then the others with large energy, savings of energy may (more than) compensate for the loss in bit rate [62]. Meanwhile, this scheme may more suitable for optical communication because the transmitted points with large probability, which have small energy, suffer less nonlinearity.

In this chapter, we propose a block-interleaved coded modulation (BICM) with iterative decoding (ID) scheme, which is suitable for arbitrary non-uniform signaling, where the information bits and parity bits transmitted with different modulation schemes but same symbol rate in order to achieve the same data rate as with conventional modulation scheme. We demonstrate the efficiency of proposed coded modulation scheme with non-uniform signaling in ASE noise dominated scenario, which represents a realistic scenario when coarse digital back propagation is combined with sliding-window turbo equalization [7]. Meanwhile, the Huffman code matched signal constellation sets (9-QAM, 12-QAM), which used for information bits transmission are also introduced in the paper. The Monte Carlo simulations indicate that the proposed LDPC-coded 9-QAM non-uniform signaling scheme with Huffman code based constellation shaping outperforms the corresponding LDPC-coded 8-QAM by 0.8 dB.

4.2 CONSTELLATION SHAPING WITH HUFFMAN CODE

The method of achieving non-uniform signaling schemes for the transmission of binary data is introduced by Kschischang [63], but not in optical communication context. In this paper, we mainly focus on the 2D 9-QAM and 12-QAM constellation sets. [64] The former one, which is shown in Figure 4.1(a), has an average bit rate of 3 bits/T, where T is the symbol duration. Each symbol can carry two, three or four bits per symbol with different probabilities. It is obvious that the center point standing for 00 has the largest probability of 0.25. The mapping rule is determined by employing the Huffman procedure shown as a tree diagram in Fig. 3. The 2D 12-QAM constellation sets shown in Figure 4.1(c), which is 16-QAM without the 4 points at the outer layer, has an average bit rate of 3.5 bits/ T. As an illustration, the received symbol constellation for ASE noise dominated channel, based on 2D-9QAM and 2D 12-QAM transmissions are shown in Figure 4.1(c) and (d). The 2D 77-QAM is shown in (e) and received constellation sets are shown in (f), which has an average bit rate of 5.718 bits/symbol.

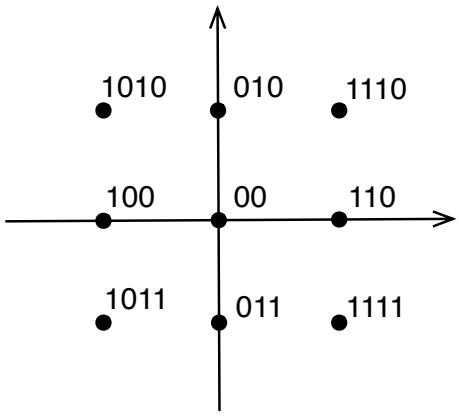

(a)

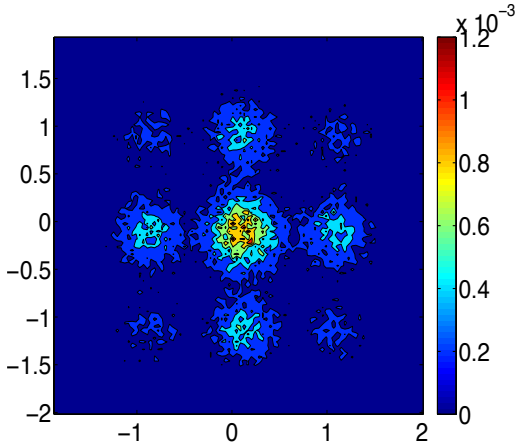

(b)

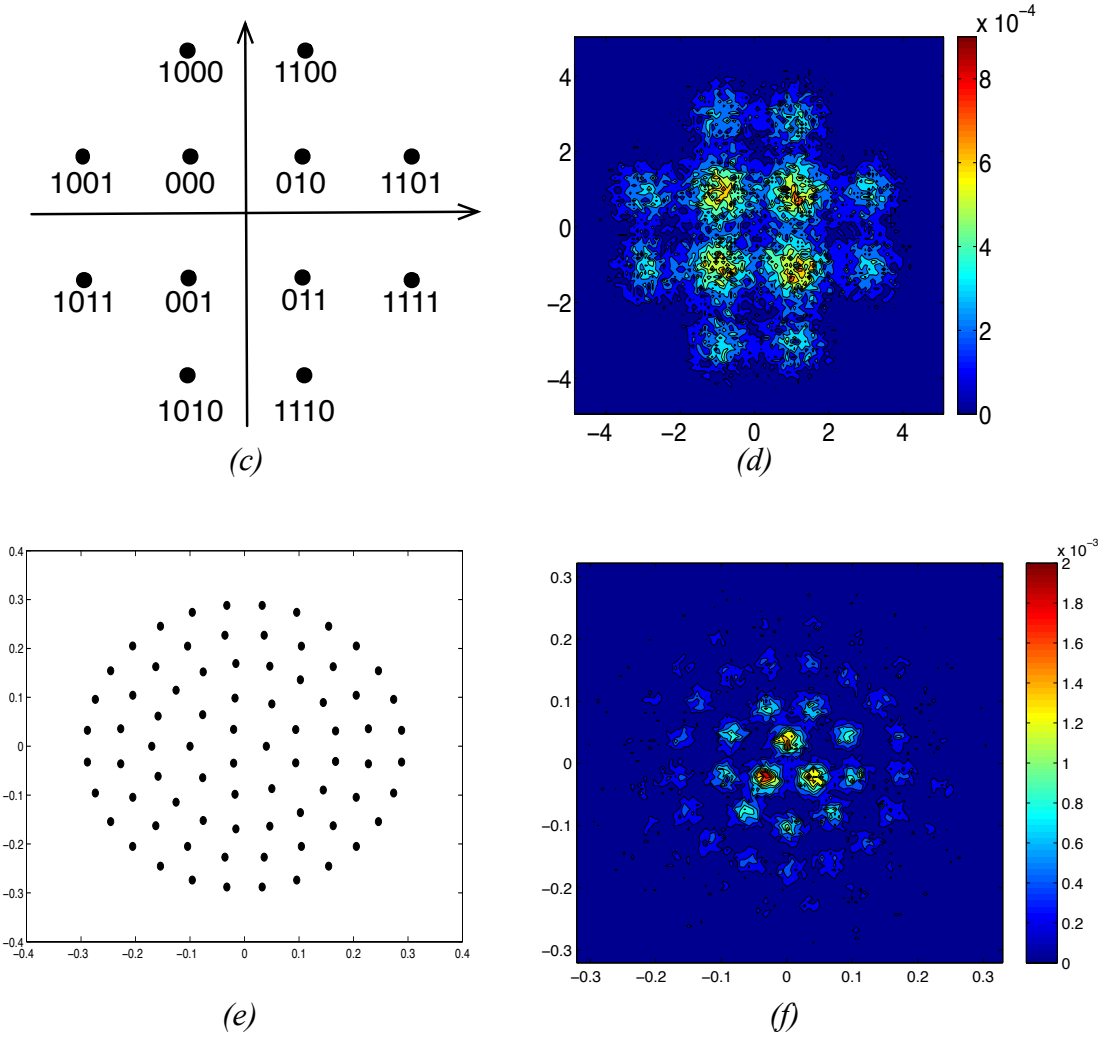

Figure 4.1 Constellation sets: (a) 2D 9-QAM, (b) received constellation of 9-QAM, (c) 2D 12-QAM, (d) received constellation of 12-QAM, (e) 2D-77QAM, (f) received constellation of 77QAM.

4.3 CONSTELLATION DESIGN FOR NON-UNIFORM SCHEME

With the statement in section 4.2, the constellation structure of the non-uniform constellation sets are decided by the structure of the binary tree or Huffman code. The constellation structure denotes the numbers of points in each layer. In order to obtain the constellation which is optimal for non-uniform signaling scheme, an overall search algorithm with the criterion of constellation

figure of merit (CFM) is used in constellation design. In any data transmission scheme, we would like to transmit at a large bit rate, with higher reliability and lower transmitter power as possible [62]. A commonly used figure of merit, named as CFM, for constellation sets is defined as follow:

$$\mathrm{CFM} \triangleq \frac{d_{min}^2}{E} \tag{4.1}$$

where d_{min} denotes the minimum distance of the constellation sets while E denotes the average energy of the constellation sets.

The proposed algorithm for non-uniform constellation design is an overall search method to determine the radius of each layer and the relative angle for each layer. As introduced above, the constellation structure has already determined by the structure of the Huffman code, so the input of the algorithm is number of points on each layer and number of layers, represented as N_i and S. The algorithm will search over all possible R_i, which denotes the radius of each layer, with a defined step size Δr. Meanwhile, the algorithm also searches over the relative angle for each layer with another step size $\Delta\theta$. After increase of each step size, the CFM will be calculated. The algorithm will keep searching over a given range of radius and angle and the combination with maximum CFM will the output of the algorithm. With the radius of each layer and the relatively angle for each layer, the constellation sets can be found with the help of N_i and S. As an illustration, the example of 9-QAM is shown in Figure 4.2.

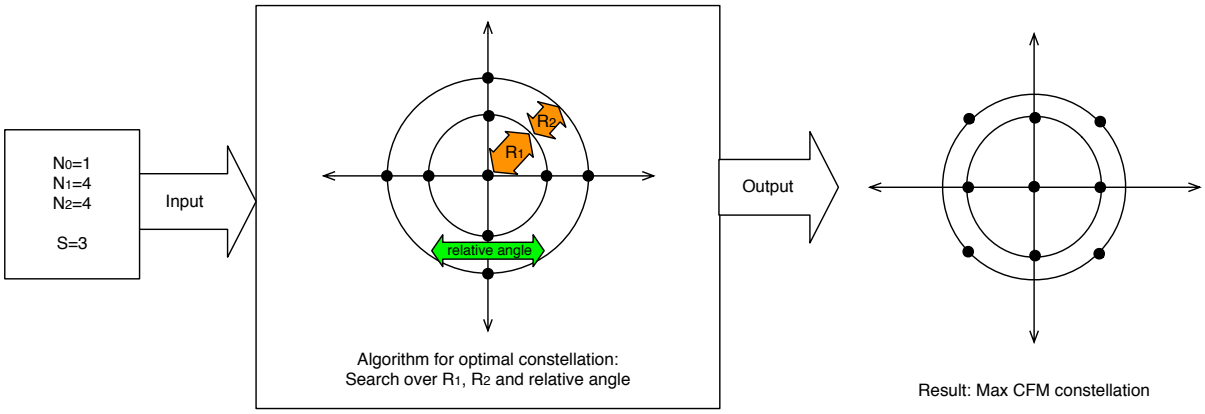

Figure 4.2 The algorithm to design the 9-QAM for non-uniform signaling

As introduced in previous section, the 9 symbols Huffman code can be represented with binary sequence: 00, 010, 110, 011, 100, 1110, 1111, 1010 and 1011. With this structure, we can find the structure of the constellation should be $N_0 = 1,\ N_1 = 4,\ N_2 = 4$ and $S = 3$. We first put one point in the center because the first layer only has one symbol, then we place 4 points on each layer. The next step would be search over all possible radius of each layer with a step size Δr and also the relative angle for second and third layer, which shows in Figure 4.2. After searching over a given range, we can find that the 3×3 square 9-QAM has the maximum CFM value. So the 9-QAM is the optimal constellation for 9 symbols non-uniform signaling.

4.4 LDPC CODED BICM-ID SCHEME FOR NON-UNIFORM SIGNALING

In this section, we introduce the proposed LDPC coded BICM-ID scheme for arbitrary non-uniform signaling in order to maintain the shaping gain brought and possibility to use the joint source channel decoding (JSCD) algorithm. As an illustration, we mainly focus on 2D-9QAM code with systematic quasi-cyclic (QC) LDPC at rate $r = 0.8$, codeword length $n = 16935$, and number of parity bits $n - k = 3385$. The key ingredient of our scheme is the structure of block-interleaver for non-uniform signaling. The conventional block interleaver of 8-QAM is shown in

Figure 4.3(a). The uniform binary data has been written in a row-wise fashion into the interleaver with the size of $(n-k)\times\log_2 M$, where M is the size of the constellation. Then each row will be encoded with the systematic LDPC code and the resulting size of the interleaver upon encoding will be $n\times\log_2 M$. At the end, each column will be mapped to one of the constellations point.

Table 4.1: The probability of each symbol and corresponding punctured bits.

Information Bits	Probability	Punctured Bits
00	0.25	01
010	0.125	0
110	0.125	1
011	0.125	0
100	0.125	1
1110	0.0625	N/A
1111	0.0625	N/A
1010	0.0625	N/A
1011	0.0625	N/A

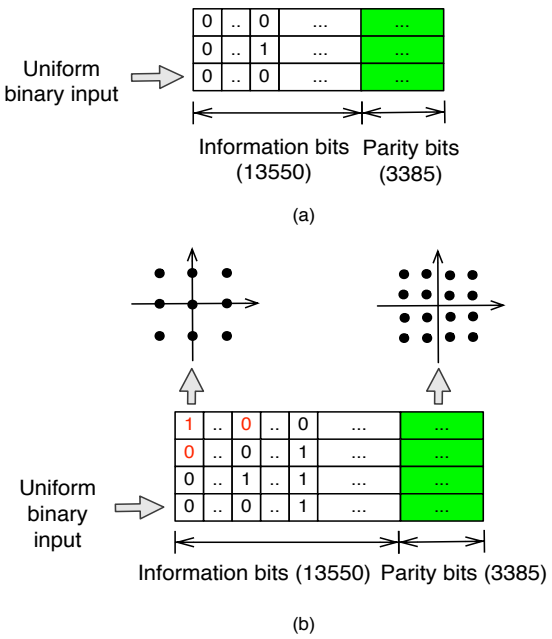

Figure 4.3 Block interleaver structure for: (a) 8-QAM, (b) 9-QAM

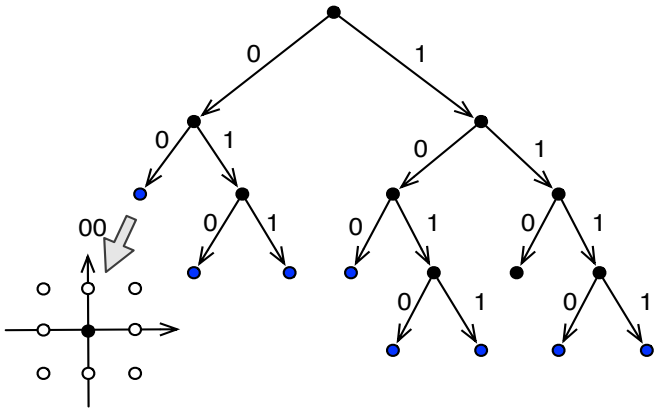

Figure 4.4 The tree representation of mapping by Huffman code of 9-QAM.

The proposed interleaver scheme suitable for non-uniform signaling is shown in Figure 4.3. Some of the locations in the proposed interleaver are filled with punctured bits summarized in Table 4.1. The interleaving process can be formulated as follows, by observing 9-QAM as an illustrative example:

- The binary information bits will be first written into the last two rows of the interleaver. The interleaver size for non-uniform signaling is $n \times L_M$, where L_M is the maximum source codeword length of the corresponding Huffman code.
- Read the bits in column-wise fashion from bottom to the top for the last two rows. If these two bits are not 00, then continue writing the information bits to the third row, otherwise leave the position blank.
- Read the bits column-wise from bottom to the top for the last three rows. If the three bits are in the set $\{101,111\}$, then continue writing the information bits to the fourth row; otherwise, leave the position blank.
- Fill the blank positions with the punctured bits according to Table 4.1.

Encode every row using the QC-LDPC encoder and generate the parity bits' blocks.

As shown in Figure 4.4, the proposed interleaver scheme requires one additional row compared to the conventional one with the purpose of maintaining the same bit rate. The bits marked as red can be considered as punctured bits only used for bit log-likelihood ratio (LLR) calculation (they are not transmitted). The parity bits in the block may not satisfy the relation in Table 4.1, which will cause the ambiguities in bit LLR calculation. To solve for this problem, the parity blocks are transmitted with 16-QAM instead of 9-QAM so that the spectral efficiency of the proposed scheme is identical to that of conventional 8-QAM. In each time frame, which corresponds to the time duration for transmitting each block, the proposed interleaver will first transmit 9-QAM information symbols followed by 16-QAM parity symbols.

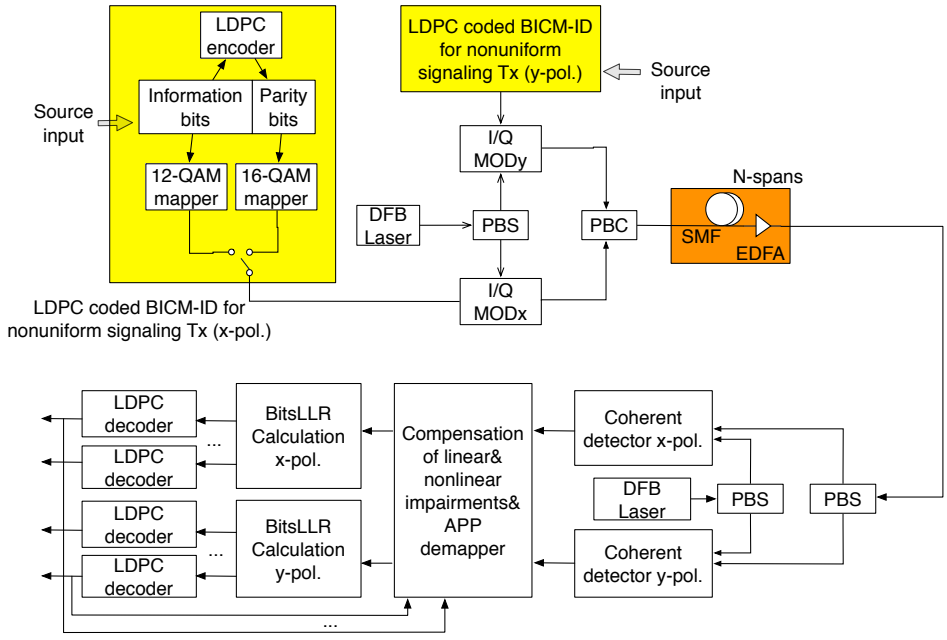

Figure 4.5 Polarization-multiplexed LDPC-coded non-uniform signaling transmission scheme. PBS/C: polarization beam splitter/combiner, MAP: maximum a posteriori probability, LLRs: log-likelihood ratios.

The entire coded modulation scheme with non-uniform signaling, suitable for use in polarization-division multiplexing (PDM), is shown in Figure 4.5. The block interleaver is filled

by the binary uniform input as well as by QC-LDPC encoder. Then the L_M bits taken from the interleaver in column-wise fashion are mapped onto the 9-QAM constellation, for the information portion, with the help of I/Q modulator. For the parity-bit portion of interleaver, the 16-QAM is used instead. Notice that the transmitter first transmits information bits with 9-QAM and then parity bits with 16-QAM at the same channel condition. The independent polarization streams are combined by polarization beam combiner and transmitted over the system of interest. On receiver side, conventional polarization-diversity receiver is used, with small number of coefficients in digital back propagation scheme, just to reduce the channel memory so that the complexity of sliding-window MAP equalizer that follows is not too high. The sliding-MAP equalizer provides soft symbol LLRs, which are used to calculate bit LLRs and further passed to LDPC decoders. The iteration between the sliding-MAP equalizer and LDPC decoder is performed until the valid codewords are generated or the maximum number of iterations is reached, which is 5 outer iterations and 20 inner iterations in our case. Regarding the LDPC decoder, the sum-product algorithm is used.

4.5 SIMULATION RESULTS

The results of Monte Carlo simulations for the proposed BICM-ID with non-uniform signaling are summarized in Figure 4.6. The symbol rate is set to Rs=31.25 GS/s. Notice that the legend "QAM9_QPSK" denotes that the information bits are transmitted by 9-QAM based on non-uniform signaling, while the parity bits are transmitted by QPSK. The "QAM9_16QAM" introduced in the previous section and "QAM8" have the same data rate, which is 2.4 bits/symbol with the consideration of code rate. It is evident that the non-uniform signaling scheme outperforms LDPC-coded 8-QAM by 0.8 dB. If we use QPSK to transmit parity bits

instead of 16-QAM, the performance can be further improved by 0.4 dB, while the average achievable information rate get reduced to 2.001 bits/symbol. Meanwhile, the QAM12_QPSK has similar performance with QAM8 but it has an average bit rate of 2.3335 bits/symbol and QAM12_QAM16 can achieve the bit rate of 2.8 bits/symbol. The QAM77_16 has an average bit rate of 3.8 bits/symbol. Note that QAM12_QPSK and QAM9_QAM16 have similar bit rate, but the latter performs better then former for 0.4dB. That means the different non-uniform schemes can achieve different shaping gains. Meanwhile, the 8QAM and QAM12_QAM16 has similar performance, but non-uniform scheme has higher bit rate.

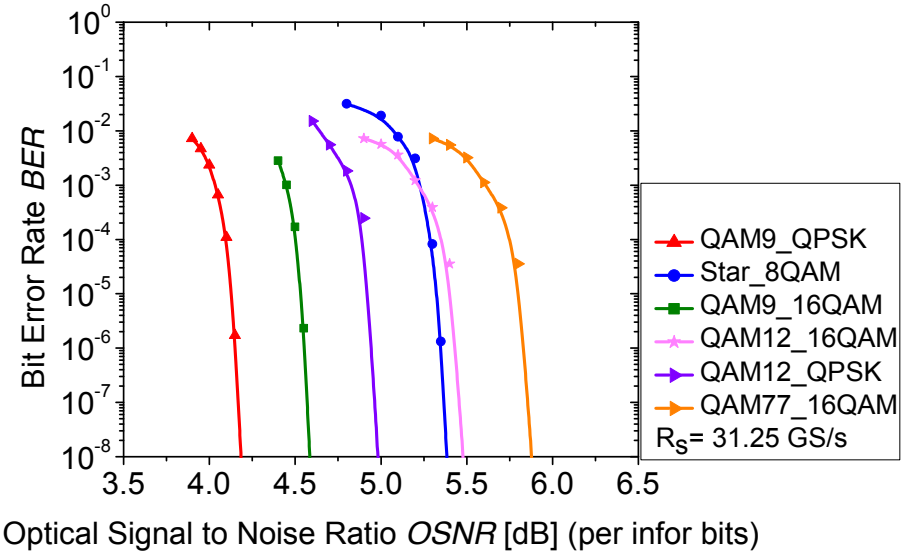

Figure 4.6 BER results of the proposed LDPC-coded non-uniform signaling scheme

4.6 CONCLUSION

In conclusion, we have proposed an LDPC coded BICM-ID scheme that is suitable for arbitrary non-uniform signaling based optical communication system. The 9-QAM and 12-QAM is used to demonstrate the efficiency of the proposed transmission scheme. The Monte Carlo simulations

indicate that the proposed non-uniform signaling scheme outperforms LDPC-coded 8-QAM by at least 0.8 dB for the same spectral efficiency.

CHAPTER 5

CONCLUSION AND FUTURE WORK

In order to improve the channel capacity and move it closer to Shannon limit, there are two approaches we can use. The first one is designing the signal constellation sets. The improvement achieved by this approach can be regarded as coding gain of the constellation design. In this dissertation, we described the optimal signal constellation design algorithm (OSCD) to achieve this goal. We first expand the OSCD algorithm to multidimensional case, which is a very popular topics these years [65]-[69], and then discover its corresponding mapping method. Because the long haul transmission system is limited by nonlinearities and XPM for DWDM system, we describe an OSCD algorithm to design the constellation that is more tolerant to either SPM or XPM. Meanwhile, we also expand the SPM case to multidimensional case. The efficiency of OSCD has already verified by the experimental demonstration and it can be considered as a competitive candidate for next generation coherent optical communication system. The other approach that can improve the channel capacity is the non-uniform signaling, which is becoming a hot topic [70]-[76] recently. Instead of transmitting every symbol equally likely, each symbol is transmitted with different probability. This approach can be considered as probability shaping for the constellation sets, which is achieved by using Huffman code or prefix code. The most important problem for non-uniform signaling is that it is hard to combine with binary LDPC code because the demapping of the signals requires the hard decision of the received symbols and makes it hard to calculate bit LLRs. In this dissertation, a new interleaver structure has been proposed. The LDPC coded modulation scheme for non-uniform signaling can adapt to any binary LDPC code. When further combining with rate-adaptive code, this scheme can fit to any data rate comparing with conventional modulation formats.

Future work of the advanced modulation formats will mainly focus on both the OSCD algorithm for more complex scenario and non-uniform signaling for more general case. To further increase

the capacity of the fiber links, OSCD can also be used in space division multiplexing system such as few-mode fiber based OFDM coherent optical transmission [77]-[82]. The nonlinearity robustness of OSCD can be estimated with post DSP symbol compensation [83]-[84]. The coded-modulation of OSCD based system can further improve by using advanced coding scheme [85]. Moreover, both OSCD and non-uniform signaling scheme can be used in CO-OFDM [86]-[88]. And the performance of the proposed scheme combined with LDPC codes also need to be verified by FPGA implementation [89]-[91]. At last, the OSCD can also used in the short distance transmission for optical metro network as GPON/EPON [92]. The future research topics can be summarized as follows.

- OSCD algorithm for free-space channel and few-mode fiber.
- Low complexity DSP algorithm for OSCD family.
- Non-uniform signaling scheme with arithmetic code.
- Non-uniform signaling combined with joint source decoding and rate adaptive LDPC code.
- Signal constellation design for non-uniform signaling scheme.

The schemes discussed above are promising pathways enabling future multi-Tb/s optical transport and multi-Tb/s Ethernet technologies.

REFERENCES

[1] P. Winzer, "Beyond 100G ethernet," *IEEE Comm. Mag*., vol. 48, pp. 26-30, 2010.

[2] I. B. Djordjevic, T. Liu, L. Xu and T. Wang. "Optimum signal constellation design for high-speed optical transmission", in Proc. *OFC/NFOEC 2012*, Paper no. OW3H.2, Mar. 6-8, 2012, Los Angeles, CA, USA.

[3] I. B. Djordjevic, M. Arabaci, L. Xu, and T. Wang, "Spatial-domain-based multidimensional modulation for multi-Tb/s serial optical transmission," *Opt. express,* vol. 19, no. 7, pp. 6845-6857, 2011.

[4] T. Cover, and J. Thomas, Elements of Information Theory, *Wiley*, 1991.

[5] H. G. Batshon, I. B. Djordjevic, L. Xu and T. Wang, "Iterative polar quantization based modulation to achieve channel capacity in ultrahigh-speed optical communication systems," *IEEE Photon. J.* vol. 2, no. 4, pp. 593-599, 2010.

[6] I. B. Djordjevic, M. Arabaci, and L. Minkov, "Next generation FEC for high-capacity communication in Optical transport network", *IEEE Photon. J.* vol. 2, no. 4, pp. 593-599, 2010.

[7] I. B. Djordjevic, L. L. Minkov, L. Xu and T. Wang, "Suppression of fiber nonlinearities and PMD in coded-modulation schemes with coherent detection by using turbo equalization," *IEEE/OSA J. Opt. Commun. Netw.,* vol. 1, no. 6, pp. 555-564, 2009.

[8] S. Zhang, T. Liu, Y. Zhang, F. Yaman, I. B. Djordjevic and T. Wang, "Optimized signal constellation for ultra-high-speed optical transport," In Proc. *SPIE 2015*, invited talk, February 7-12 2015, San Francisco, CA.

[9] T. Tanimura, Y. Koganei, H. Nakashima, T. Hoshida, and J. C. Rasmussen, "Soft decision forward error correction over nonlinear transmission of 1-Tb/s superchannel," in Proc. *ECOC*, Paper no. Th.1.3.4, September 21-25 2014, Cannes, France.

[10] H. Zhang and H. Batshon, "40Tb/s transoceanic transmission with span length of 121km and EDFA-only amplification," *OECC/ACOFT*, pp. 1–3, 2014.

[11] D. Qian, M. F. Huang, S. Zhang, Y. Zhang, Y.-K. Huang, F. Yaman, I. B. Djordjevic, and E. Mateo, "30tb/s c- and l-bands bidirectional transmission over 10,181km with 121km span length," *Opt. Express,* vol. 21, pp. 14244–14250, 2013.

[12] J. T. Rahn, S. Kumar, M. Mitchell, R. Malendevich, H. Sun, K. Wu, P. Mertz, K. Croussore, H. Wang, M. Kato, V. Lal, P. Evans, D. Lambert, H. Tsai, P. Samra, B. Taylor, A. Nilsson, S. Grubb, R. Nagarajan, F. Kish, and D. Welch, "250Gb/s real-time PIC-based super-channel transmission over a gridless 6000km terrestrial link," in Proc. *OFC/NFOEC*, 2012, Paper no. PDP5D.5, Mar. 6-8, 2012, Los Angeles, CA, USA..

[13] J. Renaudier, O. Bertran-Pardo, A. Ghazisaeidi, P. Tran, H. Mardoyan, P. Brindel, A. Voicila, G. Charlet, and S. Bigo, "Experimental transmission of Nyquist pulse shaped 4-D coded modulation using dual polar- ization 16QAM set-partitioning schemes at 28 Gbaud," in Proc. *OFC/NFOEC*, 2013, Paper no. OTU3B.1, 17-21 Mar. 2013, Anaheim, CA, USA.

[14] I. B. Djordjevic, "On the irregular nonbinary QC-LDPC-Coded hybrid multidimensional OSCD-modulation enabling beyond 100 Tb/s optical transport," *J. Lightw. Technol.,* vol. 31, pp. 2969–2975, 2013.

[15] T. Liu, I. B. Djordjevic, L.Xu and T. Wang, "Feedback channel capacity inspired optimum signal constellation design for high-speed optical transmission," in *Proc. CLEO 2012,* Paper no. CTh3C.2, 6-11 May, 2012, San Jose, CA.

[16] T. Liu and I. B. Djordjevic, "On the optimum signal constellation design for high-speed optical transport networks," *Opt. Express,* vol. 2, no. 18, pp. 20396-20406, 2012.

[17] T. Liu and I. B. Djordjevic, "Multi-dimensional optimal signal constellation sets and

symbol mappings for block-interleaved coded-modulation enabling ultra-high-speed optical transport," *IEEE Photonics Journal*, vol. 6, no. 4, pp. 5500714, 2014.

[18] T. Liu, I. B. Djordjevic, X. Lei and T. Wang, "Multidimensional optimum signal constellation design for few-mode fiber based high-speed optical transport," in *Proc. IEEE Photonics Conference 2012*, Paper no. TuM2, 23-27 September, 2012, San Francisco, CA.

[19] I. B. Djordjevic, M. Arabaci, L. Xu, and T. Wang, "Spatial-domain-based multidimensional modulation for multi-Tb/s serial optical transmission," *Opt. express*, vol. 19 no. 7, pp. 6845-6857, 2011.

[20] J. Zhang and I. B. Djordjevic, "Optimized four-dimensional mapping for high-speed optical communication systems," in Proc. *OFC/NFOEC 2012*, Paper no. OW1H.2, Mar. 6-8, 2012, Los Angeles, CA, USA.

[21] I. B. Djordjevic, and B. Vasic, "Orthogonal frequency division multiplexing for high-speed optical transmission," *Opt. express*, vol. 14, pp. 3767-3775, 2006.

[22] I. B. Djordjevic, W. Ryan, and B. Vasic, Coding for Optical Channels. Springer, 2010.

[23] S. S. Haykin, Digital Communications. Wiley, 1988.

[24] V. Ilic, T. Liu, I. B. Djordjevic, M. Li, and F. Kuppers, N. Stojanovic, "Optimal signal constellation design for nonlinear chromatic dispersion optical channel," in Proc. 12th *TELSIKS 2015*, pp. 129-132, October 14 - 17, 2015, Nis, Serbia.

[25] F. Schreckenbach, N. Gortz, J. Hagenauer, and G. Bauch, "Optimization of symbol mappings for bit-interleaved coded modulation with iterative decoding," *IEEE Commun. Lett.* vol. 7, pp. 593-595, 2003.

[26] T. Liu and I. B. Djordjevic, "EXIT chart analysis of optimal signal constellation sets and symbol mappings for block-interleaved coded-modulation enabling ultra-high-speed optical

transport," in *IEEE ICTON 2013*, June 23 -27, 2013, Cartagena, Spain.

[27] D. Zou, T. Liu, I. B. Djordjevic and T. Wang, "Optimum signal constellation design and mapping rule for few-mode fiber based LDPC-coded CO-OFDM," in *Proc. CLEO 2013*, Paper CM1G.7, June 9-14, 2013, San Jose, CA, USA.

[28] K. P. Ho, Phase modulated Optical Communication System, Springer, 2005.

[29] G. P. Agrawal, Nonlinear Fiber Optics, Academic, 2006.

[30] Hanzo, W. Webb, and T. Keller, Single- and Multi-carrier Quadrature Amplitude Modulation: Principles and Applications for Personal Communications, WLANs and Broadcasting, Wiley, 2000.

[31] P. T. Lua, and J. M. Kahn, "Signal design and detection in presence of nonlinear phase noise," *J. Lightw. Technol.*, vol. 25, no. 3, pp. 779-783, 2004.

[32] L. Beygi, E. Agrell, and M. Karlsson, "Optimization of 16-point ring constellations in the presence of nonlinear phase noise," in *Proc. OFC/NFOEC 2011*, paper OThO4, Mar. 6-10, 2011, Los Angles, CA, USA.

[33] C. Hager, A. Grell, A. Alvarado, and E. Agrell, "Design of APSK constellations for coherent optical channels with nonlinear phase noise," *IEEE Trans. Comm.,* vol. 61, no. 8, pp. 3362,3373, 2013.

[34] Shannon, C.E. (1948), "A mathematical theory of communication", *Bell System Technical Journal,* vol. 27, pp. 379–423 & 623–656, July & October, 1948.

[35] I. B. Djordjevic and T. Wang, "On the LDPC-coded modulation for ultra-high-speed optical transport in the presence of phase noise," in *Proc. OFC/NFOEC 2013*, paper OM2B.1, 17-21 Mar. 2013, Anaheim, CA, USA.

[36] Z. Tao, W. Yan, L. Liu, L. Li, S. Oda, T. Hoshida, and J. C. Rasmussen, “Simple fiber model for determination of XPM effects,” *J. Lightwave Technol.,* vol. 29, no. 7, pp. 974–986, 2011.

[37] M. Magarini, A. Spalvieri, F. Vacondio, M. Bertolini, M., and G. Gavioli, "Empirical modeling and simulation of phase noise in long-haul coherent optical transmission systems," *Opt. Express*, vol. 19, no. 23, pp. 22455-22461, 2011.

[38] G. Colavolpe, A. Barbieri, and G Caire, "Algorithms for iterative decoding in the presence of strong phase noise" *Selected Areas in Communications, IEEE Journal on,.* vol. 23, no. 9, pp. 1748-1757, 2005.

[39] M Magarini, L. Barletta, A. Spalvieri, A., Leven, M. Pepe, M., G. Gavioli, "Impact of nonideal phase reference on soft decoding of differentially encoded modulation," *Photonics Technology Letters, IEEE,* vol. 24, no. 23, pp. 2179-2182, 2012.

[40] R. J. Essiambre, et. al., “Capacity limits of optical fiber networks,” *J. Lightw. Technol*. vol. 28, no. 4, pp. 662-701, 2010.

[41] M. Sjodin, P. Johannisson, H. Wymeersch, P. Andrekson, and M. Karlsson, “Comparison of polarization-switched QPSK and polarization-multiplexed QPSK at 30 Gbit/s,” *Opt. Express*, vol. 19, no. 8, pp. 7839–7846, Apr. 2011.

[42] J. H. Conway and N. J. A. Sloane, Sphere Packings, Lattices and Groups, Springer, Dec. 1998.

[43] M. Cvijetic, Optical transmission systems engineering, Artech House, Boston, MA, 2004.

[44] T. Liu and I. B. Djordjevic, “Optimal signal constellation design for ultra-high-speed optical transport in the presence of nonlinear phase noise, ” *Opt. Express,* vol. 22, no. 26, pp. 32188-32198, Dec. 2014.

[45] G. Keiser, Optical Fiber Communications, 3rd edition, McGraw-Hill, New York, 2000.

[46] G. P Agrawal, Lightwave Technology: Telecommunication System, Wiley, New York, 2005.

[47] S. Kumar, Impact of Nonlinearities on Fiber Optic Communications. Springer, 2011.

[48] L. Beygi, E. Agrell, M. Karlsson, and P. Johannisson, "Signal statistics in fiber-optical channels with polarization multiplexing and self-phase modulation", *J. Lightw. Technol*., vol. 29, no. 16, pp. 2379–2386, Aug. 2011.

[49] I. B. Djordjevic and B. Vasic, "Multilevel coding in M-ary DPSK/differential QAM high-speed optical transmission with direct detection", *IEEE/OSA J. Lightwave Technol 24*, pp 420-428, 2006.

[50] I. B. Djordjevic, T. Liu, L. Xu and T. Wang, "Optimal signal constellation design for high-speed optical transmission", in *Proc. OFC/NFOEC 2012*, Paper no. OW3H.2, Mar. 6-8, 2012, Los Angeles, CA, USA.

[51] J. A. Angulta, J. Herreros, I. B. Djordjevic, "Coherent Multimode OAM Superpositions for Multidimensional Modulation", *IEEE Photon. J.,* vol. 6, no. 2, pp. 7900811, 2014.

[52] M. L. F. Abbade, G. H. Assis, C. J. Alves, C. A. Messani, E. A. M. Fagotto and M. Cvijetic, "All-Optical Phase and Delay Spectral Encoding of Signals with Advanced Modulation Formats", in *Proc. ICTON 2014*, Paper no. Tu.B1.4, July 6-10, 2014, Graz, Austria,

[53] L. F. Mollenauer, J. P. Gordon, and F. Heismann, "Polarization scattering by soliton-soliton collisions*," Opt. Lett.,* vol.20, no. 20, pp. 2060-2062, Oct. 1995.

[54] C. R. Menyuk and B. S. Marks, "Interaction of polarization mode dispersion and nonlinearity in optical fiber transmission systems," *J. Lightw. Technol.,* vol. 24, no. 7, pp. 2806-2826, Jul. 2006.

[55] M. Karlsson and H. Sunnerud, "Effects of nonlinearities on PMD-induced system impairments," *J. Lightw. Technol.*, vol. 24, no. 11, pp. 4127-4137, Nov. 2006.

[56] M. Winterm, C. Bunge, D. Setti, and K. Petermann, "A statistical treatment of cross-polarization modulation in DWDM systems," *J. Lightw. Technol.*, vol. 27, no. 17, pp. 3739-3751, Sep. 2009.

[57] Q. Lin and G. P. Agrawal, "Effect of polarization-mode dispersion on cross-polarization modulation in dispersion-managed wavelength-division-multiplexed systems," *J. Lightw. Technol.*, vol. 22, no. 4, pp. 977-987, Apr. 2004.

[58] JC. Palais, Fiber Communication Systems, 5th edition, Pearson Prentice Hall, 2005.

[59] R. J. Essiambre, G. Kramer, P. J. Winzer, G. J. Foschini, and B. Goebel, "Capacity limits of optical fiber networks," *J. Lightwave Technol.,* vol. 28, no. 4, pp. 662–701, 2010.

[60] M. Seimetz, High-Order Modulation for Optical Fiber Transmission, Springer (2009).

[61] J. E. Porath et al., "Design of multidimensional signal constellations," *IEEE Proc. Commun.,* vol. 150, no. 5, pp. 317-323, 2003.

[62] F. Kschischang et al., "Optimal Non-uniform Signaling for Gaussian Channels," *IEEE Trans. Inform. Theory,* vol. 39, pp. 913-929, 1993.

[63] K. Khandani et al., "Shaping Multidimensional Signal Spaces. Part I: Optimal Shaping Shell Mapping," *IEEE Trans. Inform. Theory,* vol. 39, no. 6, pp. 1799-1808, 1993.

[64] T. Liu, I. B. Djordjevic, "LDPC-coded BICM-ID with nonuniform signaling for ultra-high-speed optical transport," in Proc. *ACP 2015*, Paper AM3F.3, 19 - 23 November 2015, Hong Kong.

[65] M. Karlsson and E. Agrell, "Multidimensional optimized modulation for- mats", Ch. 2 in "Enabling Technologies for High Spectral efficiency Coherent Optical Communication

Networks," ed. X. Zhou and C. Xie, Wiley, 2016, to appear.

[66] J. Viterbi, "On coded phase-coherent communications", *IRE Trans. Space El. and Telem.* , SET-7, pp. 3–14, 1961.

[67] G. D. Forney, "Multidimensional constellations—Part I: Introduction, figures of merit, and generalized cross constellations", *IEEE J. Sel. Areas Commun.,* vol. 7, pp. 877–892, 1989.

[68] M. Karlsson and E. Agrell, "Which is the most power-efficient modulation format in optical links?", *Opt. Express,* vol. 17, pp. 10814–10819, 2009.

[69] Alvarado and E. Agrell, "Four dimensional coded modulation with bit- wise decoders for future optical communications", *J. Lightw. Technol.*. vol. 33, pp. 1993–2003, 2015.

[70] G. Böcherer, "Probabilistic signal shaping for bit-metric decoding," in Proc. *IEEE Int. Symp. Inf. Theory*, pp. 431-435, 2014

[71] X. Zhou, L. E. Nelson, P. Magill, R. Isaac, B. Zhu, D. W. Peckham, P. I. Borel and K. Carlson, "High spectral efficiency 400 Gb/s transmission using PDM time-domain hybrid 32-64 QAM and training-assisted carrier recovery", *J. Lightw. Technol.,* vol. 31, no. 7, pp. 999-1005, 2013

[72] L. Nadal, M. S. Moreolo, J. M. Fàbrega, A. Dochhan, H. Grießer, M. Eiselt and J.-P. Elbers, "DMT modulation with adaptive loading for high bit rate transmission over directly detected optical channels", *J. Lightw. Technol.,* vol. 32, no. 21, pp. 4143-4153, 2014.

[73] R. Dar, M. Feder, A. Mecozzi and M. Shtaif, "On shaping gain in the nonlinear fiber-optic channel," in Proc. *IEEE Int. Symp. Inf. Theory,* pp. 2794-2798, 2014.

[74] B. Smith and F. Kschischang, "A pragmatic coded modulation scheme for high-spectral-efficiency fiber-optic communications", *J. Lightw. Technol*., vol. 30, no. 13, pp. 2047-2053, 2012.

[75] M. Yankov, D. Zibar, K. Larsen, L. Christensen and S. Forchhammer, "Constellation shaping for fiber-optic channels with QAM and high spectral efficiency", *IEEE Photon. Technol. Lett.,* vol. 26, no. 23, pp. 2407-2410, 2014.

[76] P. Schulte and G. Böcherer, "Constant composition distribution matching", *IEEE Trans. Inf. Theory*, vol. 62, no. 1, pp. 420-434, 2016.

[77] Changyu Lin, Ivan B. Djordjevic, Milorad Cvijetic, and Ding Zou, "Mode-Multiplexed Multi-Tb/s Superchannel Transmission with Advanced Multidimensional Signaling in the Presence of Fiber Nonlinearities," *IEEE Trans. on Comm.*, vol. 62, no. 7, pp. 2507-2514, July 2014.

[78] Changyu Lin, Ivan B. Djordjevic and et al., "Non-binary LDPC Coded Mode-multiplexed Coherent Optical OFDM 1.28 Tbit/s 16-QAM Signal Transmission over 2000-km of Few-mode Fibers with Mode Dependent Loss," *IEEE Photon. J.*, Oct. 2012.

[79] Ding Zou, Changyu Lin and Ivan B. Djordjevic, "LDPC-Coded Mode-Multiplexed CO-OFDM over 1000 km of Few-Mode Fiber," in Proc. *CLEO 2012*, San Jose, CA, May 2012.

[80] Changyu Lin, Ivan B. Djordjevic and Milorad Cvijetic "Quantum Few-Mode Fiber Communications Based on the Orbital Angular Momentum," *IEEE Photon. Technol. Lett.*, Jan. 2013.

[81] Changyu Lin, Ivan B. Djordjevic and et al., "Nonbinary LDPC-Coded OFDM over Four/Eight-Mode Fibers with Mode-Dependent Loss," in Proc. *IEEE Photonics Conference* 2012, Paper 598-599, San Francisco, CA, 2012.

[82] I. B. Djordjevic, M. Cvijetic, and Changyu Lin, "Multidimensional Signaling and Coding Enabling Multi-Tb/s Optical Transport and Networking," *IEEE Sig. Proc. Mag.,* Vol.31, No.2, Mar. 2014.

[83] Changyu Lin, Ivan B. Djordjevic, Ding Zou, "Achievable Information Rates Calculation for Optical OFDM Transmission over Few-mode fiber Long-haul Transmission Systems," *Opt. Express*, vol. 23, no. 13, pp. 16846-16856, 2015.

[84] Changyu Lin, Sethumadhavan Chandrasekhar, Peter J. Winzer, "Experimental Study of the Limits of Digital Nonlinearity Compensation in DWDM Systems," In Proc. OFC 2015, paper Th4D.4, Mar. 2015, Los Angeles, CA, USA.

[85] Changyu Lin, Ivan B. Djordjevic and et al. "Tandem-turbo-product Nonbinary BICM for Next-generation High-speed Optical Transmission Systems," in Proc. *OFC 2016*, Paper Th1D.5, Mar. 2016, Anaheim, CA, USA.

[86] D. Zou, I. B. Djordjevic, "Multi-Tb/s Optical Transmission based on Polarization-Multiplexed LDPC-coded Multi-band OFDM," in Proc. *ICTON 2011*, Paper 1-4, June 2011, Stockholm, Sweden.

[87] D. Zou, I. B. Djordjevic, "Beyond 1Tb/s Superchannel Optical Transmission based on Polarization Multiplexed Coded-OFDM over 2300 km of SSMF," in Proc. *SPPCom 2012*, Paper SpTu2A.6, June 2012, Colorado Springs, CO, USA.

[88] I. B. Djordjevic, D. Zou, and M. Cvijetic, "Hybrid Multidimensional Dynamic Optical Networking based on Adaptive LDPC-Coded Mode-Multiplexed CO-OFDM," in Proc. ACP 2012, Paper 1-4, 7-10 Nov. 2012, Guangzhou, China.

[89] D. Zou, I. B. Djordjevic, "FPGA-based Non-binary QC-LDPC Coding for High-Speed Coherent Optical Transmission," in Proc. *CLEO 2015*, Paper 1-2, May 2015, San Jose, CA, USA.

[90] D. Zou, I. B. Djordjevic, "FPGA implementation of concatenated non-binary QC-LDPC codes for high-speed optical transport," *Opt. Express*, vol. 23, no. 10, pp. 14501-14509, May 2015.

[91] D. Zou, I. B. Djordjevic, "An FPGA design of generalized low-density parity-check codes for rate-adaptive optical transport networks," in Proc. *Photonics West 2016*, OPTO, Paper 9773-22, Feb. 2016, San Francisco, CA, USA.

[92] M. Tao, L. Zhou, S. Yao, D. Zou, S. Li, H. Lin, X. Liu, "28Gb/s TDM-PON with narrow filter compensation and enhanced FEC supporting 31.5dB link loss budget after 20-km downstream transmission," in Proc. OFC 2016, Paper Th1l.4, Mar. 2016, Anaheim, CA, USA.